PHYSICAL REVIEW D **94,** 114031 (2016)

Quasielastic production of polarized hyperons in antineutrino-nucleon reactions

F. Akbar, M. Rafi Alam, M. Sajjad Athar,* and S. K. Singh

Department of Physics, Aligarh Muslim University, Aligarh-202002, India

(Received 6 August 2016; published 27 December 2016)

We have studied the differential cross section as well as the longitudinal and perpendicular components of polarization of the final hyperon (Λ,Σ) produced in the antineutrino induced quasielastic charged current reactions on nucleon and nuclear targets. The nucleon-hyperon transition form factors are determined from the experimental data on quasielastic ($\Delta S = 0$) charged current (anti)neutrino-nucleon scattering and the semileptonic decay of neutron and hyperons assuming G-invariance, T-invariance, and SU(3) symmetry. The vector transition form factors are obtained in terms of nucleon electromagnetic form factors for which various parametrizations available in the literature have been used. A dipole parametrization for the axial vector form factor and the pseudoscalar transition form factor derived in terms of the axial vector form factor assuming PCAC and GT relation extended to the strangeness sector has been used in numerical evaluations. The flux averaged cross section and polarization observables corresponding to the CERN Gargamelle experiment have been calculated for quasielastic hyperon production and found to be in reasonable agreement with the experimental observations. The numerical results for the flux averaged differential cross section $\frac{d\sigma}{dQ^2}$ and longitudinal (perpendicular) polarization $P_L(Q^2)(P_P(Q^2))$ relevant for the antineutrino fluxes of MINERνA, MicroBooNE, and T2K experiments have been presented. This will be useful in interpreting future experimental results on production cross sections and polarization observables from the experiments on the quasielastic production of hyperons induced by antineutrinos and exploring the possibility of determining the axial vector and pseudoscalar form factors in the strangeness sector.

DOI: 10.1103/PhysRevD.94.114031

I. INTRODUCTION

Our knowledge of the transition form factors in the antineutrino induced quasielastic process of hyperon production ($|\Delta S| = 1$) is far from satisfactory. Recently, with the development of high intensity (anti)neutrino beams in the few GeV region, considerable interest has developed in understanding these weak transition form factors especially in the axial vector sector. These form factors have been determined experimentally and theoretically using Cabibbo theory assuming SU(3) symmetry and other symmetries of weak hadronic currents in the Standard Model. Most of these form factors are determined from the analysis of semileptonic decay of hyperons and neutron which are limited to very low momentum transfer. These form factors are found to be consistent with SU(3) symmetry which relates them to the form factors in the $\Delta S = 0$ sector of (anti)neutrino-nucleon scattering and to the various couplings in semileptonic hyperon decays. However, the status of G-invariance, conservation of vector current(CVC), partial conservation of axial current(PCAC), etc. which seem to work quite well in the nucleon sector, are not well understood when extended to the octet of baryons using SU(3) symmetry which is known to be an approximate symmetry. Even though the vast amount of data available on semileptonic decay of hyperons is consistent with the assumption of SU(3) symmetry, the violation of G-invariance and SU(3) symmetry is not ruled out [1]. There is no unambiguous way to implement SU(3) symmetry as far as CVC and PCAC are concerned, but the prescriptions which have been used in the literature to implement the symmetry seem to work well [1–3].

The charged current quasielastic production of hyperons by antineutrinos (charged current quasielastic production induced by neutrinos is prohibited by the $\Delta S = \Delta Q$ rule, while any neutral current production induced by ν and $\bar{\nu}$ is prohibited by the absence of flavor changing neutral current (FCNC) in the Standard Model) is the most appropriate place to study the nucleon-hyperon transition form factors which enables us to extend the study of form factors to higher Q^2 beyond the Q^2 values accessible in semileptonic hyperon decays. There are some experimental studies performed to determine these form factors from the cross section measurements done for these processes at CERN [4–6], BNL [7], FNAL [8,9], and Serpukhov [10] which are limited by low statistics. Theoretically, these reactions have been studied for more than 50 years [11–21], but recently, there has been renewed interest in studying these reactions [22–27] due to the feasibility of doing experiments with the availability of high intensity antineutrino beams [28–33].

*sajathar@gmail.com

Most of the theoretical calculations have been done only for the production cross section, but there exist some calculations also for the polarization of the produced hyperons [13–18]. There is only one experiment done at CERN which has reported the results for the polarization observables for Λ hyperon produced in the quasielastic $\bar{\nu}_\mu p \to \mu^+ \Lambda$ reaction [6].

Experimentally, there is now a possibility to study the production cross section of hyperons and other strange particles as well as polarization of hyperons at present facilities at Fermilab [28] and J-PARC [29] where high intensity beams of (anti)neutrinos are available. The experiments planned with liquid argon TPC (LArTPC) detectors at MicroBooNE [30] and ArgoNeuT [31] and the proposed DUNE [32] and LAr1-ND, ICARUS-T600 [34] experiments at Fermilab will be able to see charged hadrons in coincidence, thus making it possible to measure polarization in addition to the cross section measurements being done at MINERνA [33]. It is, therefore, the most appropriate time to theoretically perform the calculations for the polarization observables in addition to the differential cross sections in the Standard Model using Cabibbo theory and/or quark models, using the present state of knowledge about the symmetry of weak hadronic currents and the properties of transition form factors associated with the matrix element between the hadronic states. Since these experiments are planned to be performed using nuclear targets, it is important that we understand the implications of nuclear medium effects in the interpretation of the experimental results. This will facilitate the analysis of experimental results when they become available. We propose to study theoretically the production and polarization of hyperons produced in the following reactions:

$$\begin{aligned} \bar{\nu}_\mu + p &\to \mu^+ + \Lambda \\ \bar{\nu}_\mu + p &\to \mu^+ + \Sigma^0 \\ \bar{\nu}_\mu + n &\to \mu^+ + \Sigma^-, \end{aligned} \tag{1}$$

on nucleons and nuclear targets using Cabibbo theory in the Standard Model with the GIM mechanism for extension to strangeness sector. We also assume the T-invariance and the absence of second class currents which forbid the existence of hyperon polarization perpendicular to the reaction plane.

In Sec. II, we describe in brief the formalism for calculating the cross section and polarization of hyperons produced in the quasielastic antineutrino reactions on free and bound nucleons. The effect of nuclear medium arising due to Fermi motion and Pauli blocking of initial nucleon states are also considered. We have in this paper not taken into account the final state interaction effect of outgoing polarized hyperons, the work for which is in progress and will be reported elsewhere. In Sec. III, we present the results and discussion and give the summary and conclusions in Sec. IV.

II. FORMALISM

A. Matrix element and transition form factors

The transition matrix element for the process

$$\bar{\nu}_\mu(k) + N(p) \to \mu^+(k') + Y(p'), \qquad (N = p, n; Y = \Lambda, \Sigma)$$

depicted in Fig. 1, is written as

$$\mathcal{M} = \frac{G_F}{\sqrt{2}} \sin\theta_c l^\mu [\bar{u}_Y(p') J_\mu u_N(p)]. \tag{2}$$

In the above expression G_F is the Fermi coupling constant and θ_c is the Cabibbo angle. Here, l^μ is the leptonic current given by

$$l^\mu = \bar{u}(k')\gamma^\mu(1+\gamma_5)u(k), \tag{3}$$

and J_μ is the hadronic current operator given by

$$J_\mu = V_\mu - A_\mu, \tag{4}$$

where

$$V_\mu = \gamma_\mu f_1^{NY}(Q^2) + i\sigma_{\mu\nu}\frac{q^\nu}{m_N + m_Y} f_2^{NY}(Q^2) + \frac{q_\mu}{m_N + m_Y} f_3^{NY}(Q^2) \tag{5}$$

and

$$A_\mu = \gamma_\mu\gamma_5 g_1^{NY}(Q^2) + i\sigma_{\mu\nu}\gamma_5\frac{q^\nu}{m_N + m_Y} g_2^{NY}(Q^2) + \frac{q_\mu}{m_N + m_Y} g_3^{NY}(Q^2)\gamma_5. \tag{6}$$

Here, m_N and m_Y are the masses of initial and final baryons, respectively, and $q_\mu (= p'_\mu - p_\mu)$ is the four momentum transfer with $Q^2 = -q^2$, $Q^2 \geq 0$. The six form factors $f_i^{NY}(Q^2)$ and $g_i^{NY}(Q^2)$ $(i = 1\text{–}3)$ are determined using following assumptions about the vector and axial vector currents in weak interactions:

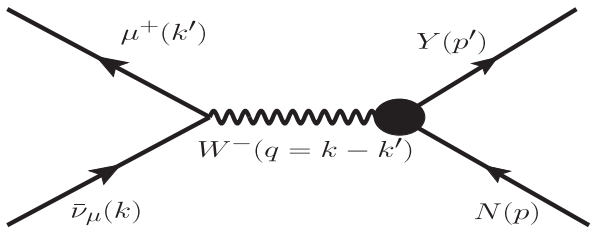

FIG. 1. Feynman diagram for the process $\bar{\nu}_\mu(k) + N(p) \to \mu^+(k') + Y(p')$, where N and Y stand for initial nucleon and final hyperon, respectively. The quantities in the bracket represent four momentum of the corresponding particles.

(a) The assumptions of T-invariance, G-invariance, and SU(3) symmetry have been used to determine all the form factors $f_i^{NY}(Q^2)$ and $g_i^{NY}(Q^2)$ defined in Eqs. (5) and (6), respectively.

(b) For the determination of vector form factors, we have assumed CVC which leads to $f_3^{NY}(Q^2)=0$. The remaining two vector form factors $f_1^{NY}(Q^2)$ and $f_2^{NY}(Q^2)$ are determined in terms of the electromagnetic form factors of nucleon, i.e., $f_1^N(Q^2)$ and $f_2^N(Q^2)$, and are tabulated in Table I for different processes given in Eq. (1). The electromagnetic form factors of the nucleon, i.e., $f_1^N(Q^2)$ and $f_2^N(Q^2)$, are in turn written in terms of Sach's electric ($G_E^{p,n}(Q^2)$) and magnetic ($G_M^{p,n}(Q^2)$) form factors. The details are given in Ref. [27].

There are various parametrizations for the vector form factors given in literature [35–42]. We use the parametrization given by Bradford *et al.* [35] known as BBBA05 in all the numerical calculations presented here except in the case of $\bar{\nu}_\mu n \to \mu^+\Sigma^-$, where sensitivity of our results to the charge form factor of neutron $G_E^n(Q^2)$ is discussed, and parameterizations of $G_E^n(Q^2)$ due to Galster *et al.* [36,37] and Kelly [38] have also been considered.

(c) In the axial vector sector, the form factor $g_2^{NY}(Q^2)$ vanishes due to G-invariance, T-invariance, and SU(3) symmetry, and the axial vector form factor $g_1^{NY}(Q^2)$ is given in terms of the axial form factor $g_A(Q^2)$ corresponding to $n \to p$ transitions. Here, x is a parameter which describes the ratio of symmetric and antisymmetric coupling in the analysis of hyperon semileptonic decays (HSD) and is determined phenomenologically from the experimental data [1]. For each reaction considered in this work [Eq. (1)], the form factor $g_1^{NY}(Q^2)$ is given in Table I. A dipole parametrization for $g_A(Q^2)$ has been used with axial dipole mass M_A, i.e.,

$$g_A(Q^2) = g_A(0)\left(1+\frac{Q^2}{M_A^2}\right)^{-2}, \tag{7}$$

with $g_A(0)=1.2723$ determined from data on the β decay of neutron [43]. The numerical value of dipole mass M_A used in this work is discussed in Sec. II(f) below.

(d) The pseudoscalar form factor $g_3^{NY}(Q^2)$ is obtained in terms of the axial vector form factor $g_1^{NY}(Q^2)$ assuming PCAC and Goldberger-Treiman (GT) relation extended to the strangeness sector. We use expressions given by Marshak *et al.* [17] and Nambu [44] where further details can be found. Explicitly, in our numerical calculations we use the following expressions for the pseudoscalar form factor $g_3^{NY}(Q^2)$:

(i) Marshak *et al.* [17]:

$$g_3^{NY}(Q^2) = \frac{(m_N+m_Y)^2}{Q^2} \times \left(\frac{g_1^{NY}(Q^2)(m_K^2+Q^2)-m_K^2 g_1^{NY}(0)}{m_K^2+Q^2}\right), \tag{8}$$

(ii) Nambu [44]:

$$g_3^{NY}(Q^2) = \frac{(m_N+m_Y)^2}{(m_K^2+Q^2)} g_1^{NY}(Q^2), \tag{9}$$

with m_K being the mass of kaon and $g_1^{NY}(Q^2)$ for different NY transitions is given in terms of $g_A(Q^2)$ defined in Eq. (7).

(e) We see from Table I that SU(3) symmetry predicts a simple relation between the vector and axial vector form factors for reactions $\bar{\nu}_\mu p \to \mu^+\Sigma^0$ and $\bar{\nu}_\mu n \to \mu^+\Sigma^-$, which implies that

$$\left[\frac{d\sigma}{dQ^2}\right]_{\bar{\nu}_\mu p\to\mu^+\Sigma^0} = \frac{1}{2}\left[\frac{d\sigma}{dQ^2}\right]_{\bar{\nu}_\mu n\to\mu^+\Sigma^-} \tag{10}$$

and

$$[P_{L,P}]_{\bar{\nu}_\mu p\to\mu^+\Sigma^0} = [P_{L,P}]_{\bar{\nu}_\mu n\to\mu^+\Sigma^-}. \tag{11}$$

It should be emphasized that these relations and other implications of SU(3) symmetry and G-invariance can be tested in the strangeness sector with the availability of precise data on weak hyperon production induced by antineutrinos.

(f) The numerical value of the axial dipole mass (M_A) to be used in the calculations of neutrino-nucleus cross section is a subject of intense discussion in the neutrino physics community, and a wide range of M_A has been recently discussed in the literature [45–47]. The old data available on (anti)neutrino scattering on hydrogen and deuterium targets [48–50] reanalyzed by Bodek *et al.* [51] gives a value of

TABLE I. Vector and axial vector from factors for $\bar{\nu}_\mu(k)+N(p)\to\mu^+(k')+Y(p')$ processes.

	$f_1^{NY}(Q^2)$	$f_2^{NY}(Q^2)$	$g_1^{NY}(Q^2)$
$\bar{\nu}_\mu p\to\mu^+\Lambda$	$-\sqrt{\frac{3}{2}}f_1^p(Q^2)$	$-\sqrt{\frac{3}{2}}f_2^p(Q^2)$	$-\frac{1}{\sqrt{6}}(1+2x)g_A(Q^2)$
$\bar{\nu}_\mu n\to\mu^+\Sigma^-$	$-[f_1^p(Q^2)+2f_1^n(Q^2)]$	$-[f_2^p(Q^2)+2f_2^n(Q^2)]$	$(1-2x)g_A(Q^2)$
$\bar{\nu}_\mu p\to\mu^+\Sigma^0$	$-\frac{1}{\sqrt{2}}[f_1^p(Q^2)+2f_1^n(Q^2)]$	$-\frac{1}{\sqrt{2}}[f_2^p(Q^2)+2f_2^n(Q^2)]$	$\frac{1}{\sqrt{2}}(1-2x)g_A(Q^2)$

$M_A = 1.014 \pm 0.014$ GeV, while a recent analysis of the same data by Meyer *et al.* [52] gives a value in the range of 1.02–1.17 GeV depending upon which data of ANL [48], BNL [49], and FNAL [50] experiments are considered. Previously, all the world data on quasielastic (anti)neutrino scattering from nuclear targets were analyzed by Bernard *et al.* [53] to yield $M_A = 1.026 \pm 0.021$ GeV.

In recent years, high statistics data on quasielastic neutrino-nucleus scattering have been obtained and analyzed from neutrino and antineutrino scattering on nuclear targets both at low and intermediate energies. The data from NOMAD [54] and MINERνA [33] favor a lower value of M_A around 1.03 GeV, while the data from MiniBooNE [55], MINOS [56], K2K [57], T2K [58], and SciBooNE [59,60] favor a higher value of M_A which lies in the range of 1.2–1.35 GeV. It is argued that at lower energies corresponding to these experiments, the (anti)neutrino quasielastic scattering from nuclear targets like ^{12}C and ^{16}O are substantially affected by the nuclear medium effects arising due to meson exchange currents (MEC), multinucleon correlations leading to 2p-2h, and higher excitations in the nuclear medium. If these effects are adequately taken into account, the low energy data can also be explained by the lower value of M_A around 1.03 GeV [45–47]. Recently, an analysis of the MiniBooNE [55] and MINERνA [33] data has been done by Wilkinson *et al.* [61] which concludes that these two experimental results can be explained with the inclusion of nuclear medium effects using a value of M_A lying between 1.07–1.33 GeV. Furthermore, in a recent study Ankowski *et al.* [62] have analyzed experimental data from accelerator neutrinos on neutrino induced reaction cross section on several nuclear targets by considering a relativistic spectral function with 2p-2h effects and found that with $M_A \sim 1.2$ GeV the data on differential scattering cross section can be well explained. More recently, the data on quasielastic cross section from MiniBooNE and MINERνA have been analyzed by Stowell *et al.* [63] using NEUT and NuWro CCQE + 2p2h models, and it has been inferred that $M_A \sim 1.15$ GeV can explain these experimental data.

Keeping in view this scenario regarding the numerical values of M_A needed to explain the quasielastic cross sections in $\Delta S = 0$ (anti)neutrino-nucleus scattering, we have varied the value of M_A between 1.026–1.2 GeV in this paper to study the $|\Delta S| = 1$ quasielastic antineutrino reactions on nuclear targets. *A priori*, there is no reason to assume the same value of M_A for antineutrino quasielastic reactions in $\Delta S = 0$ and $|\Delta S| = 1$ sectors as argued by Gaillard and Sauvage [2] and supported by Cabibbo *et al.* [1]. However, this range of M_A also accommodates the suggestion of Gaillard and Sauvage [2] that the value of M_A to be used in $|\Delta S| = 1$ quasielastic reactions should be rescaled upwards by a factor $\frac{m_K^*}{m_\rho}$ (m_K^* and m_ρ are the masses of K^* and ρ mesons, respectively) over the M_A used in $\Delta S = 0$ reactions if effects of minimal SU(3) breaking are to be simulated by taking realistic hyperons and other masses in the theory of HSD.

B. Cross section

The differential cross section corresponding to the processes given in Eq. (1) may be written as

$$d\sigma = \frac{1}{(2\pi)^2}\frac{1}{4E_{\bar{\nu}_\mu} m_N}\delta^4(k + p - k' - p') \times \frac{d^3k'}{2E_{k'}}\frac{d^3p'}{2E_{p'}}\sum\bar{\sum}|\mathcal{M}|^2, \tag{12}$$

where $\mathcal{M}$ is the transition matrix element, the square of which may be written in terms of hadronic and leptonic tensors as

$$|\mathcal{M}|^2 = \frac{G_F^2 \sin^2\theta_c}{2}\mathcal{J}^{\alpha\beta}\mathcal{L}_{\alpha\beta}. \tag{13}$$

The hadronic and leptonic tensors are given by

$$\mathcal{J}^{\alpha\beta} = \mathrm{Tr}[\Lambda(p')J^\alpha\Lambda(p)\tilde{J}^\beta]$$
$$\mathcal{L}_{\alpha\beta} = \mathrm{Tr}[\gamma_\alpha(1+\gamma_5)k\!\!/\gamma_\beta(1+\gamma_5)(k'\!\!/ + m_\mu)], \tag{14}$$

with $\tilde{J}_\beta = \gamma^0 J_\beta^\dagger \gamma^0$ and $\Lambda(p) = p\!\!/ + m_N$. Using the above definitions, the Q^2 distribution is written as

$$\frac{d\sigma}{dQ^2} = \frac{G_F^2 \sin^2\theta_c}{8\pi m_N E_{\bar{\nu}_\mu}^2}\mathcal{N}(Q^2, E_{\bar{\nu}_\mu}), \tag{15}$$

where the expression of $\mathcal{N}(Q^2, E_{\bar{\nu}_\mu})$ is given in the Appendix.

When the reactions shown in Eq. (1) take place on nucleons which are bound in the nucleus, the neutrons and protons are not free, and their momenta $p_{n,p}(r)$ at r are constrained to satisfy the Pauli principle, i.e., $p_{n,p}(r) < p_{F_{n,p}}(r)$, where $p_{F_n}(r)$ and $p_{F_p}(r)$ are the local Fermi momenta of neutrons and protons at the interaction point in the nucleus and are given by $p_{F_n}(r) = [3\pi^2\rho_n(r)]^{\frac{1}{3}}$ and $p_{F_p}(r) = [3\pi^2\rho_p(r)]^{\frac{1}{3}}$, $\rho_n(r)$ and $\rho_p(r)$ are the neutron and proton nuclear densities given by $\rho_n(r) = \frac{(A-Z)}{A}\rho(r)$ and $\rho_p(r) = \frac{Z}{A}\rho(r)$, and $\rho(r)$ is the nuclear density which is determined from electron-nucleus scattering experiments.

The differential scattering cross section for the scattering of antineutrinos from nucleons in the nucleus is then given as

$$\left[\frac{d^2\sigma}{dE_l d\Omega_l}\right]_{\bar{\nu}_\mu A} = 2\int_{r_{\min}}^{r_{\max}} d^3r \int_0^{p_{F_N}(r)} \frac{d^3p}{(2\pi)^3} \times n_N(p,r)\left[\frac{d^2\sigma}{dE_l d\Omega_l}\right]_{\bar{\nu}_\mu N}, \quad (16)$$

where $n_N(p,r)$ is the local occupation number of the initial nucleon of momentum p at a radius r in the nucleus, which is 1 for $p < p_{F_N}(r)$ and 0 otherwise, and $n_N(p,r)$ is related to the density as

$$\rho = \frac{N}{V} = 2\int \frac{d^3p}{(2\pi)^3} n_N(p,r). \quad (17)$$

In the next section, we discuss briefly the construction of the polarization vector for the final hyperon.

C. Polarization of hyperons

Using the covariant density matrix formalism, polarization 4-vector (ξ^τ) of the final hyperon produced in reaction (2) is written as [64]

$$\xi^\tau = \frac{\mathrm{Tr}[\gamma^\tau\gamma_5\rho_f(p')]}{\mathrm{Tr}[\rho_f(p')]}, \quad (18)$$

where the final spin density matrix $\rho_f(p')$ is given by

$$\rho_f(p') = \mathcal{L}^{\alpha\beta}\Lambda(p')J_\alpha\Lambda(p)\tilde{J}_\beta\Lambda(p'). \quad (19)$$

Using the following relations [65,66],

$$\Lambda(p')\gamma^\tau\gamma_5\Lambda(p') = 2m_Y\left(g^{\tau\sigma} - \frac{p'^\tau p'^\sigma}{m_Y^2}\right)\Lambda(p')\gamma_\sigma\gamma_5 \quad (20)$$

and

$$\Lambda(p')\Lambda(p') = 2m_Y\Lambda(p'), \quad (21)$$

ξ^τ defined in Eq. (18) may be rewritten as

$$\xi^\tau = \left(g^{\tau\sigma} - \frac{p'^\tau p'^\sigma}{m_Y^2}\right)\frac{\mathcal{L}^{\alpha\beta}\mathrm{Tr}[\gamma_\sigma\gamma_5\Lambda(p')J_\alpha\Lambda(p)\tilde{J}_\beta]}{\mathcal{L}^{\alpha\beta}\mathrm{Tr}[\Lambda(p')J_\alpha\Lambda(p)\tilde{J}_\beta]}. \quad (22)$$

Note that in Eq. (22) ξ^τ is manifestly orthogonal to p'^τ, i.e., $p'\cdot\xi = 0$. Moreover, the denominator is directly related to the differential cross section given in Eq. (15).

With $\mathcal{J}^{\alpha\beta}$ and $\mathcal{L}_{\alpha\beta}$ given in Eq. (14), an expression for ξ^τ is obtained. In the lab frame where the initial nucleon is at rest, the polarization vector $\vec{\xi}$ is calculated to be

$$\frac{d\sigma}{dQ^2}\vec{\xi} = \frac{G_F^2\sin^2\theta_c}{8\pi m_N m_Y E_{\bar{\nu}_\mu}^2}[(\vec{k}+\vec{k}')m_Y\mathcal{A}(Q^2,E_{\bar{\nu}_\mu}) + (\vec{k}-\vec{k}')\mathcal{B}(Q^2,E_{\bar{\nu}_\mu})], \quad (23)$$

where the expressions of $\mathcal{A}(Q^2,E_{\bar{\nu}_\mu})$ and $\mathcal{B}(Q^2,E_{\bar{\nu}_\mu})$ are given in the Appendix.

From Eq. (23), it follows that the polarization lies in the scattering plane defined by $\vec{k}$ and $\vec{k}'$, and there is no component of polarization in a direction orthogonal to the scattering plane. This is a consequence of T-invariance which makes the transverse polarization in a direction perpendicular to the reaction plane vanish [16,18]. We now expand the polarization vector $\vec{\xi}$ along two orthogonal directions, $\vec{e}_L$ and $\vec{e}_P$, in the reaction plane corresponding to parallel and perpendicular directions to the momentum of the hyperon,[1] i.e.,

$$\vec{e}_L = \frac{\vec{p}'}{|\vec{p}'|} = \frac{\vec{q}}{|\vec{q}|}, \quad \vec{e}_P = \vec{e}_L\times\vec{e}_T, \quad \vec{e}_T = \frac{\vec{k}\times\vec{k}'}{|\vec{k}\times\vec{k}'|}, \quad (24)$$

and write

$$\vec{\xi} = \xi_P\vec{e}_P + \xi_L\vec{e}_L, \quad (25)$$

such that the longitudinal and perpendicular components of the polarization vector ($\vec{\xi}$) in the lab frame are given by

$$\xi_L(Q^2) = \vec{\xi}\cdot\vec{e}_L, \qquad \xi_P(Q^2) = \vec{\xi}\cdot\vec{e}_P. \quad (26)$$

From Eq. (26), the longitudinal and perpendicular components of the polarization vector $P_L(Q^2)$ and $P_P(Q^2)$ defined in the rest frame of recoil nucleon are given by [65]:

$$P_L(Q^2) = \frac{m_Y}{E_{p'}}\xi_L(Q^2), \qquad P_P(Q^2) = \xi_P(Q^2), \quad (27)$$

where $\frac{m_Y}{E_{p'}}$ is the Lorentz boost factor along $\vec{p}'$. With the help of Eqs. (23), (24), (26), and (27), the longitudinal component $P_L(Q^2)$ is calculated to be

$$\frac{d\sigma}{dQ^2}P_L(Q^2) = \frac{G_F^2\sin^2\theta_c}{8\pi|\vec{q}|E_{p'}m_N E_{\bar{\nu}_\mu}^2}[(E_{\bar{\nu}_\mu}^2 - E_\mu^2 + m_\mu^2)m_Y\mathcal{A}(Q^2,E_{\bar{\nu}_\mu}) + |\vec{q}|^2\mathcal{B}(Q^2,E_{\bar{\nu}_\mu})], \quad (28)$$

where in the lab frame $E_{p'} = \sqrt{|\vec{q}^2| + m_Y^2}$. Similarly, the perpendicular component $P_P(Q^2)$ of the polarization 3-vector is given as

[1]It should be noted that our $\vec{e}_P$ is defined as in Bilenky and Christova [65] and is opposite to the sign used by Erriquez *et al.* [4].

$$\frac{d\sigma}{dQ^2}P_P(Q^2) = -\frac{G_F^2\sin^2\theta_c}{4\pi}\frac{|\vec{k}'|}{|\vec{q}|}\frac{\mathcal{A}(Q^2,E_{\bar{\nu}_\mu})\sin\theta}{m_N E_{\bar{\nu}_\mu}}, \tag{29}$$

where θ is the scattering angle in the lab frame.

Inside the nucleus, the target nucleon is not at rest but moves with Fermi momentum, i.e., $\vec{p} \neq 0$. Because of this, the polarization components of the final hyperon get modified to

$$[P_{L,P}(Q^2)]_{\bar{\nu}_\mu A} = 2\int d^3r \int \frac{d^3p}{(2\pi)^3} n_N(p,r)[P_{L,P}(Q^2,\vec{p})]_{\bar{\nu}_\mu N}, \tag{30}$$

with longitudinal component

$$\begin{aligned} P_L(Q^2,\vec{p}) = {} & \frac{m_Y}{E_{p'}}\frac{G_F^2\sin^2\theta_c}{2}\frac{1}{|\mathcal{M}|^2}\frac{1}{|\vec{p}+\vec{q}|} \\ & \times[\alpha(Q^2,\vec{p})(\vec{k}\cdot\vec{p}+E_{\bar{\nu}_\mu}^2-\vec{k}\cdot\vec{k}') \\ & +\beta(Q^2,\vec{p})(\vec{k}'\cdot\vec{p}+\vec{k}\cdot\vec{k}'-|\vec{k}'|^2) \\ & +\eta(Q^2,\vec{p})(|\vec{p}|^2+\vec{p}\cdot\vec{q})], \end{aligned} \tag{31}$$

and perpendicular component

$$\begin{aligned} P_P(Q^2,\vec{p}) = {} & \frac{G_F^2\sin^2\theta_c}{2}\frac{1}{|\mathcal{M}|^2}\frac{1}{|\vec{p}+\vec{q}||\vec{k}||\vec{k}'|\sin\theta} \\ & \times[(\vec{k}'\cdot\vec{p}+\vec{k}\cdot\vec{k}'-|\vec{k}'|^2)\{\alpha(Q^2,\vec{p})E_{\bar{\nu}_\mu}^2 \\ & +\beta(Q^2,\vec{p})\vec{k}\cdot\vec{k}'+\eta(Q^2,\vec{p})\vec{k}\cdot\vec{p}\} \\ & -(\vec{k}\cdot\vec{p}+E_{\bar{\nu}_\mu}^2-\vec{k}\cdot\vec{k}')\{\alpha(Q^2,\vec{p})\vec{k}\cdot\vec{k}' \\ & +\beta(Q^2,\vec{p})|\vec{k}'|^2+\eta(Q^2,\vec{p})\vec{k}'\cdot\vec{p}\}]. \end{aligned} \tag{32}$$

The expressions of $\alpha(Q^2,\vec{p})$, $\beta(Q^2,\vec{p})$, and $\eta(Q^2,\vec{p})$ are given in the Appendix.

III. RESULTS AND DISCUSSION

A. Differential cross section $\frac{d\sigma}{dQ^2}$ and polarization components $P_L(Q^2)$ and $P_P(Q^2)$ for nucleon target

We have used Eqs. (15), (28), and (29) to numerically evaluate the differential cross section $\frac{d\sigma}{dQ^2}$ and longitudinal $P_L(Q^2)$ and perpendicular $P_P(Q^2)$ components of the polarization of hyperons in the quasielastic antineutrino reactions given in Eq. (1). For the vector and axial vector form factors, we have used the expressions of $f_i^{NY}(Q^2)(i=1,2)$ and $g_1^{NY}(Q^2)$ given in Table I along with the pseudoscalar form factor $g_3^{NY}(Q^2)$ given in Eqs. (8) and (9). The Q^2 dependence of the nucleon form factors $f_{1,2}^{p,n}$ is taken from the parametrization of BBBA05 [35]. A dipole parametrization for the axial vector form factor $g_A(Q^2)$ given in Eq. (7) has been used for $g_{1,3}^{NY}(Q^2)$ with $g_A(0) = 1.2723$ [43], $x = 0.364$ [1], and axial dipole mass $M_A = 1.026$, 1.1, and 1.2 GeV as mentioned in each figure.

In Fig. 2, we present the results of $\frac{d\sigma}{dQ^2}$, $P_L(Q^2)$, and $P_P(Q^2)$ for the reaction $\bar{\nu}_\mu p \to \mu^+\Lambda$ at $E_{\bar{\nu}_\mu} = 1$ GeV and in Fig. 3 at $E_{\bar{\nu}_\mu} = 3$ GeV. We see that while there is very little sensitivity of $\frac{d\sigma}{dQ^2}$ to the variation of M_A, the components of polarization $P_L(Q^2)$ and $P_P(Q^2)$ are quite sensitive to the value of M_A especially in the region $Q^2 > 0.4$ GeV^2. It should, therefore, be possible to independently determine the value of M_A from the polarization measurements. However, the present available data on the total cross section for the single hyperon production are consistent with $M_A = 1.026$ GeV [27]. At higher values of Q^2, the sensitivity of $P_L(Q^2)$ and $P_P(Q^2)$ to M_A increases, but quantitatively, the cross section $\frac{d\sigma}{dQ^2}$ decreases, making the

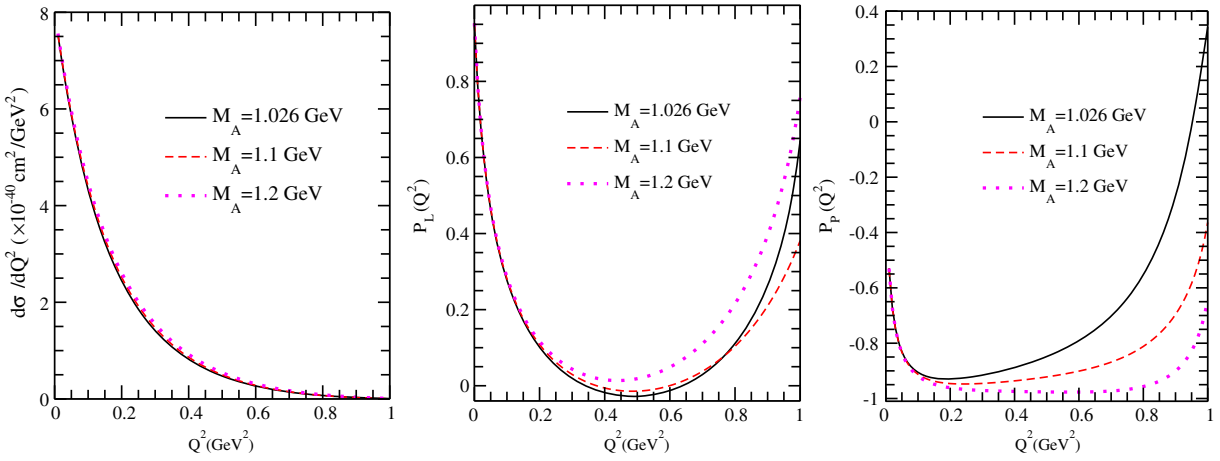

FIG. 2. Here are $\frac{d\sigma}{dQ^2}$, $P_L(Q^2)$, and $P_P(Q^2)$ vs Q^2 for the process $\bar{\nu}_\mu p \to \mu^+\Lambda$ at $E_{\bar{\nu}_\mu} = 1$ GeV for different values of M_A used in $g_1^{p\Lambda}(Q^2)$ viz. 1.026 GeV (solid line), 1.1 GeV (dashed), and 1.2 GeV (dotted line) with $m_\mu = 0$. $f_1^{p\Lambda}(Q^2)$, $f_2^{p\Lambda}(Q^2)$, and $g_1^{p\Lambda}(Q^2)$ from Table I and BBBA05 parametrization for nucleon form factor are used.

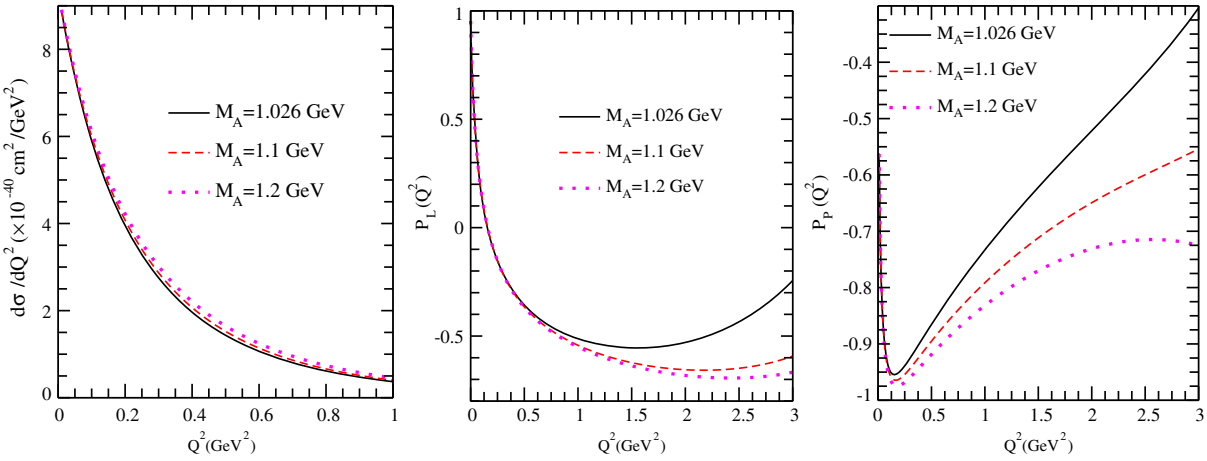

FIG. 3. Here are $\frac{d\sigma}{dQ^2}$, $P_L(Q^2)$, and $P_P(Q^2)$ vs Q^2 for the process $\bar{\nu}_\mu p \to \mu^+\Lambda$ at $E_{\bar{\nu}_\mu} = 3$ GeV for different values of M_A in $g_1^{p\Lambda}(Q^2)$. Lines and points have the same meaning as in Fig. 2.

number of events quite small and the measurement of polarization observables becomes difficult. We have also studied the sensitivity of our results for $\frac{d\sigma}{dQ^2}$, $P_L(Q^2)$, and $P_P(Q^2)$ to various other parametrizations of Q^2 dependence of the nucleon form factors $f_{1,2}^{p,n}(Q^2)$ available in the literature [35–42]. It is found that at $E_{\bar{\nu}_\mu} = 1$ GeV the results for $\frac{d\sigma}{dQ^2}$, $P_L(Q^2)$, and $P_P(Q^2)$ are not very sensitive to the choice of other parametrizations of vector form factors in the case of $\bar{\nu}_\mu p \to \mu^+\Lambda$ and are not shown in these figures.

In Figs. 4 and 5, we present the results of $\frac{d\sigma}{dQ^2}$, $P_L(Q^2)$, and $P_P(Q^2)$ for the reaction $\bar{\nu}_\mu n \to \mu^+\Sigma^-$ at $E_{\bar{\nu}_\mu} = 1$ GeV and $E_{\bar{\nu}_\mu} = 3$ GeV, respectively. The results for $\frac{d\sigma}{dQ^2}$, $P_L(Q^2)$, and $P_P(Q^2)$ are qualitatively similar to $\bar{\nu}_\mu p \to \mu^+\Lambda$ as far as the sensitivity to M_A is concerned. However, the differential cross sections $\frac{d\sigma}{dQ^2}$ are smaller, and the components of the hyperon polarization are of the same order as in reaction $\bar{\nu}_\mu p \to \mu^+\Lambda$ but slightly higher in magnitude. We have chosen to show the results for $\bar{\nu}_\mu n \to \mu^+\Sigma^-$ as the cross section for this process is larger by a factor of 2 as compared to $\bar{\nu}_\mu p \to \mu^+\Sigma^0$. While there is very little sensitivity of $\frac{d\sigma}{dQ^2}$, $P_L(Q^2)$, and $P_P(Q^2)$ to the vector form factors in the case of $\bar{\nu}_\mu p \to \mu^+\Lambda$, this is not the case for $\bar{\nu}_\mu n \to \mu^+\Sigma^-$. In the case of $\bar{\nu}_\mu n \to \mu^+\Sigma^-$ process, the results for differential cross section $\frac{d\sigma}{dQ^2}$ and polarization components $P_L(Q^2)$ and $P_P(Q^2)$ are found to be sensitive to the vector form factors especially to the neutron form factors $f_{1,2}^n(Q^2)$ occurring in the expressions of $f_{1,2}^{n\Sigma^-}$ (see Table I). This arises mainly due to the presence of the charge form factor of neutron $G_E^n(Q^2)$ in the definition of $f_{1,2}^n(Q^2)$. We have, therefore, studied the sensitivity of our results to various parametrizations of the charge form factor

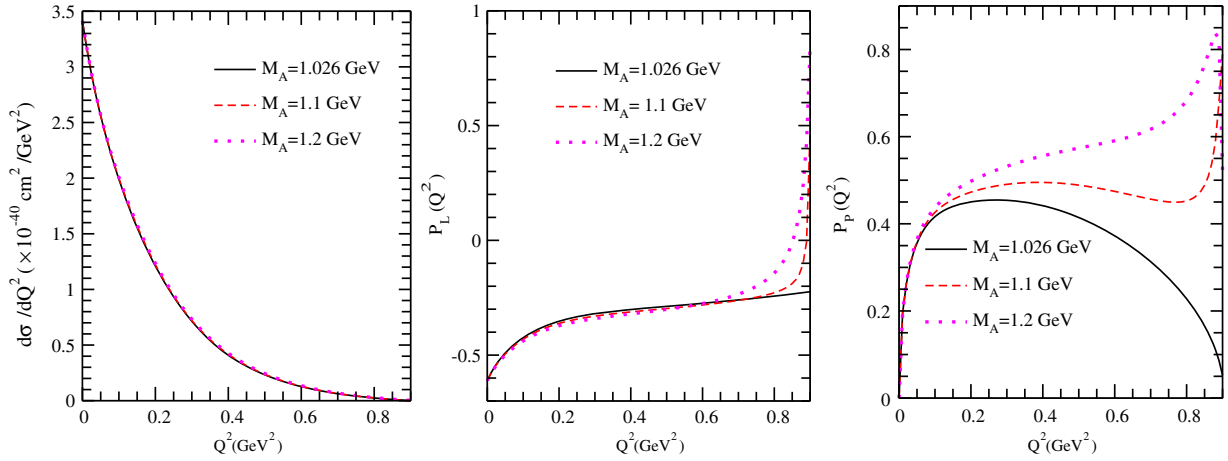

FIG. 4. Here are $\frac{d\sigma}{dQ^2}$, $P_L(Q^2)$, and $P_P(Q^2)$ vs Q^2 for the process $\bar{\nu}_\mu n \to \mu^+\Sigma^-$ at $E_{\bar{\nu}_\mu} = 1$ GeV for different values of M_A in $g_1^{n\Sigma^-}(Q^2)$. Lines and points have the same meaning as in Fig. 2.

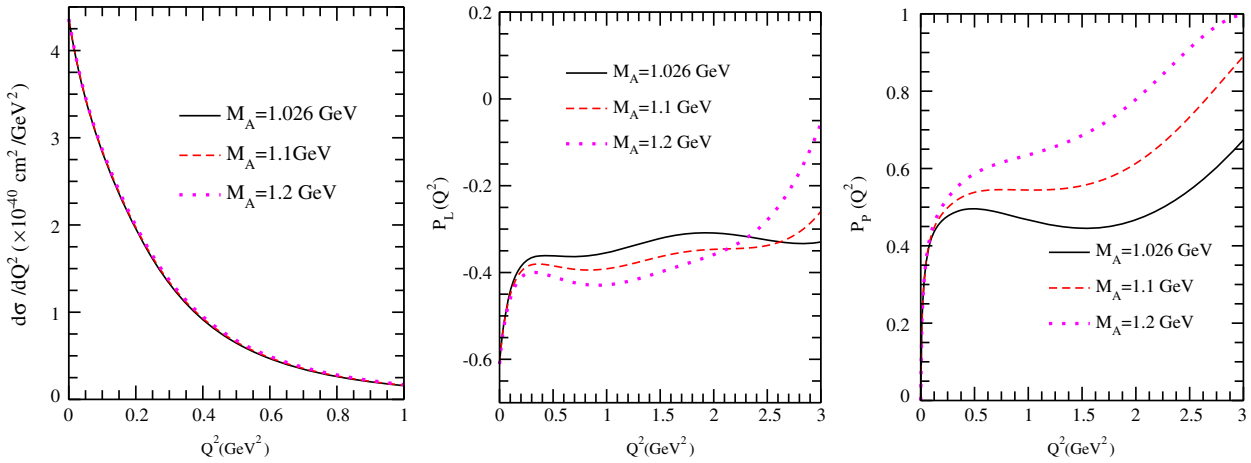

FIG. 5. Here are $\frac{d\sigma}{dQ^2}$, $P_L(Q^2)$, and $P_P(Q^2)$ vs Q^2 for the process $\bar{\nu}_\mu n \to \mu^+\Sigma^-$ at $E_{\bar{\nu}_\mu} = 3$ GeV for different values of M_A in $g_1^{n\Sigma^-}(Q^2)$. Lines and points have the same meaning as in Fig. 2.

of the neutron available in the literature. Some of the different parametrizations for $G_E^n(Q^2)$ being used recently in the literature are [35–38]:

(i) Bradford *et al.* (BBBA05) [35]:

$$G_E^n(Q^2) = \frac{a_1\tau + a_2\tau^2}{1 + b_1\tau + b_2\tau^2 + b_3\tau^3}, \tag{33}$$

with $a_1 = 1.25$, $a_2 = 1.30$, $b_1 = -9.86$, $b_2 = 305.0$, and $b_3 = 7.54$.

(ii) Galster *et al.* [36]:

$$G_E^n(Q^2) = -\frac{\mu_n\tau}{1 + 5.6\tau} G_D(Q^2), \tag{34}$$

with $\mu_n = -1.913$, $\tau = \frac{Q^2}{4m_N^2}$, $G_D(Q^2) = (1 + \frac{Q^2}{M_V^2})^{-2}$; $M_V = 0.84$ GeV.

(iii) Modified form of $G_E^n(Q^2)$ in Galster *et al.* parametrization [37]:

$$G_E^n(Q^2) = -\frac{a\mu_n\tau}{1 + b\tau} G_D(Q^2), \tag{35}$$

with $a = 1.51$ and $b = 8.4$.

(iv) Modified form of $G_E^n(Q^2)$ in Kelly parametrization [38]:

$$G_E^n(Q^2) = \frac{G_M^n(Q^2)}{\mu_n} \frac{a_1\tau}{1 + a_2\sqrt{\tau} + a_3\tau}, \tag{36}$$

with $a_1 = 2.6316$, $a_2 = 4.118$, and $a_3 = 0.29516$.

We show in Figs. 6 ($E_{\bar{\nu}_\mu} = 1$ GeV) and 7 ($E_{\bar{\nu}_\mu} = 3$ GeV), the dependence of $\frac{d\sigma}{dQ^2}$, $P_L(Q^2)$, and $P_P(Q^2)$ on the different parametrization of $G_E^n(Q^2)$. It is seen that the polarization observables are quite sensitive to

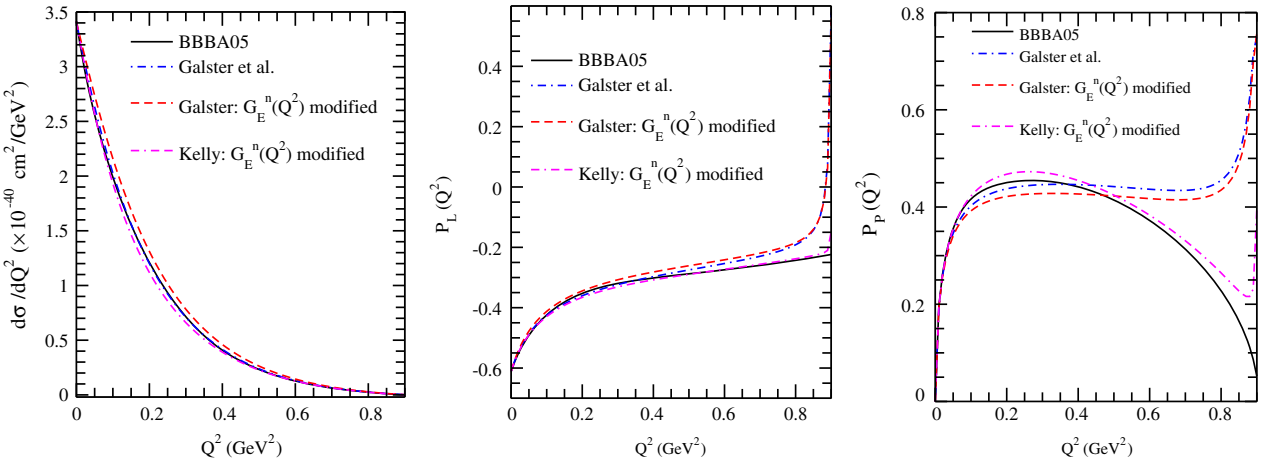

FIG. 6. Here are $\frac{d\sigma}{dQ^2}$, $P_L(Q^2)$, and $P_P(Q^2)$ vs Q^2 at $E_{\bar{\nu}_\mu} = 1$ GeV for the $\bar{\nu}_\mu n \to \mu^+\Sigma^-$ process. The results are presented with the nucleon form factors using BBBA05 [35] (solid line), Galster *et al.* [36](dashed-dotted line), modified form of $G_E^n(Q^2)$ in Galster parametrization [37] (dashed line), and modified form of $G_E^n(Q^2)$ in Kelly parametrization [38] (double dashed-dotted line).

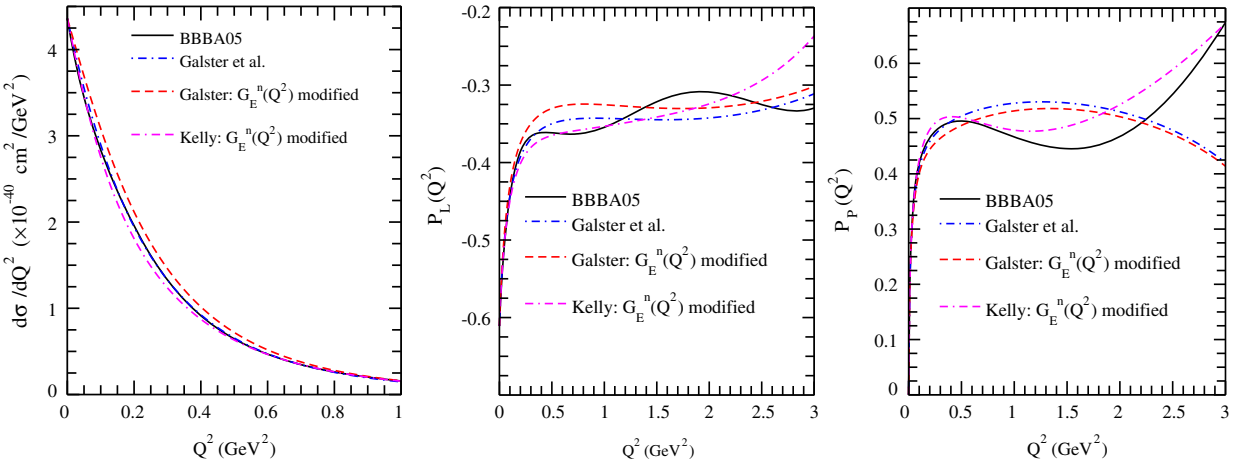

FIG. 7. Here are $\frac{d\sigma}{dQ^2}$, $P_L(Q^2)$, and $P_P(Q^2)$ vs Q^2 at $E_{\bar{\nu}_\mu} = 3$ GeV for $\bar{\nu}_\mu n \to \mu^+\Sigma^-$ process. Lines and points have the same meaning as Fig. 6.

the neutron charge form factor in $\bar{\nu}_\mu n \to \mu^+\Sigma^-$ especially at $E_{\bar{\nu}_\mu} = 3$ GeV, and it should be possible to determine, in principle, the charge form factor of neutron from the observation of $P_L(Q^2)$ and $P_P(Q^2)$ using this process.

We have made an attempt to explore the possibility of determining the pseudoscalar form factor $g_3^{NY}(Q^2)$ in the $|\Delta S| = 1$ sector by including two models for $g_3^{NY}(Q^2)$ based on PCAC and the corresponding Goldberger-Treiman relation in the strangeness sector using the parametrizations given in Eqs. (8) (Marshak *et al.* [17]) and (9) (Nambu [44]). In Figs. 8 and 9, we show the effect of $g_3^{NY}(Q^2)$ on $\frac{d\sigma}{dQ^2}$, $P_L(Q^2)$, and $P_P(Q^2)$ calculated for the processes $\bar{\nu}_\mu p \to \mu^+\Lambda$ and $\bar{\nu}_\mu n \to \mu^+\Sigma^-$, respectively, at $E_{\bar{\nu}_\mu} = 1$ GeV. We see from Figs. 8 and 9 that at $E_{\bar{\nu}_\mu} = 1$ GeV sensitivity of the cross section $\frac{d\sigma}{dQ^2}$, or the polarization observables $P_L(Q^2)$ and $P_P(Q^2)$ to the pseudoscalar form factor, $g_3^{NY}(Q^2)$ is quite small. However, at smaller antineutrino energies like $E_{\bar{\nu}_\mu} = 0.5$ GeV, the polarization components $P_L(Q^2)$ and $P_P(Q^2)$ are quite sensitive to the value of the pseudoscalar form factor as shown in Figs. 10 and 11. It seems, therefore, possible, in principle, to determine the pseudoscalar form factor in the hyperon polarization measurements at lower energies relevant for the MicroBooNE [30] and T2K [58] flux of antineutrinos.

B. Differential cross section $\frac{d\sigma}{dQ^2}$ and polarization components $P_L(Q^2)$ and $P_P(Q^2)$ for nuclear target

In Figs. 12–15, we present the results in nuclei for differential cross section $\frac{d\sigma}{dQ^2}$, longitudinal ($P_L(Q^2)$), and

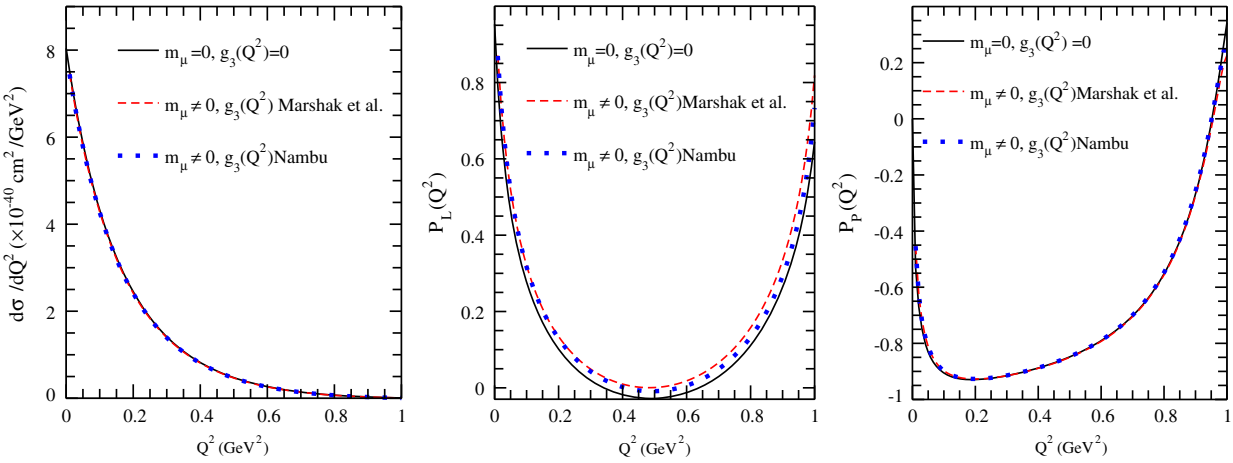

FIG. 8. Here are $\frac{d\sigma}{dQ^2}$, $P_L(Q^2)$ and $P_P(Q^2)$ vs Q^2 ($M_A = 1.026$ GeV) for the process $\bar{\nu}_\mu p \to \mu^+\Lambda$ at $E_{\bar{\nu}_\mu} = 1$ GeV using $f_1^{p\Lambda}(Q^2), f_2^{p\Lambda}(Q^2), g_1^{p\Lambda}(Q^2)$ from Table I and BBBA05 [35] parametrization for the nucleon form factors, with $m_\mu = 0$ and $g_3^{p\Lambda} = 0$ (solid line), $m_\mu \neq 0$ and $g_3^{p\Lambda} \neq 0$ from Marshak *et al.* [17] given in Eq. (8) (dashed line) and $m_\mu \neq 0$ and $g_3^{p\Lambda} \neq 0$ from Nambu [44] given in Eq. (9) (dotted line).

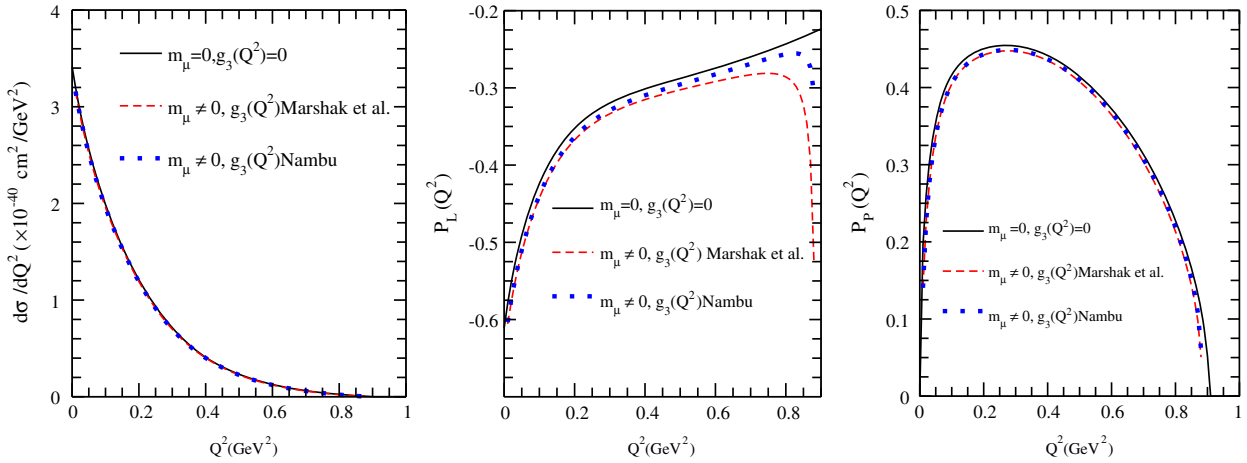

FIG. 9. Here are $\frac{d\sigma}{dQ^2}$, $P_L(Q^2)$, and $P_P(Q^2)$ vs Q^2 at $E_{\bar{\nu}_\mu} = 1$ GeV for the $\bar{\nu}_\mu n \to \mu^+\Sigma^-$ process. Lines and points have the same meaning as in Fig. 8.

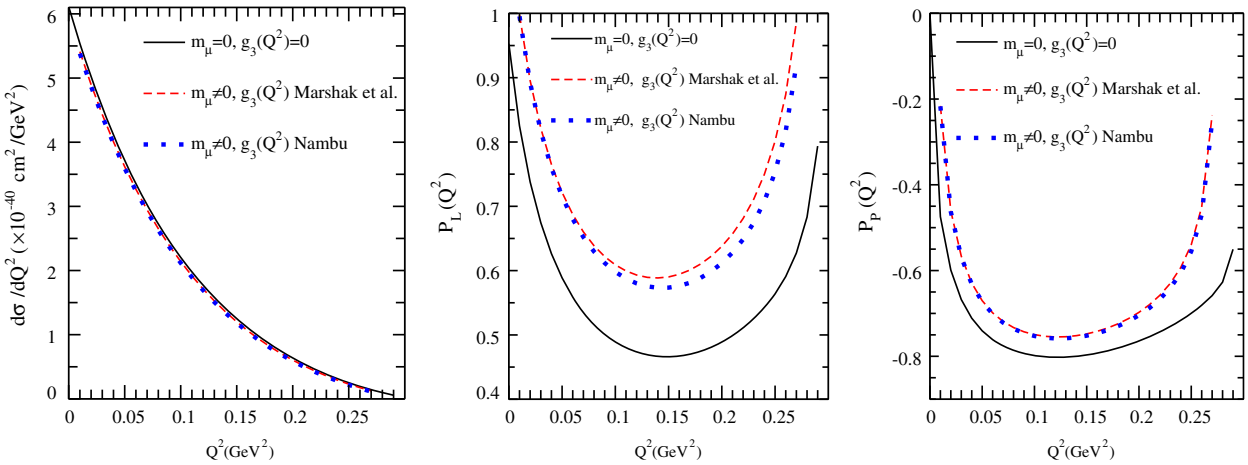

FIG. 10. Here are $\frac{d\sigma}{dQ^2}$, $P_L(Q^2)$, and $P_P(Q^2)$ vs Q^2 for the process $\bar{\nu}_\mu p \to \mu^+\Lambda$ at $E_{\bar{\nu}_\mu} = 0.5$ GeV. Lines and points have the same meaning as in Fig. 8.

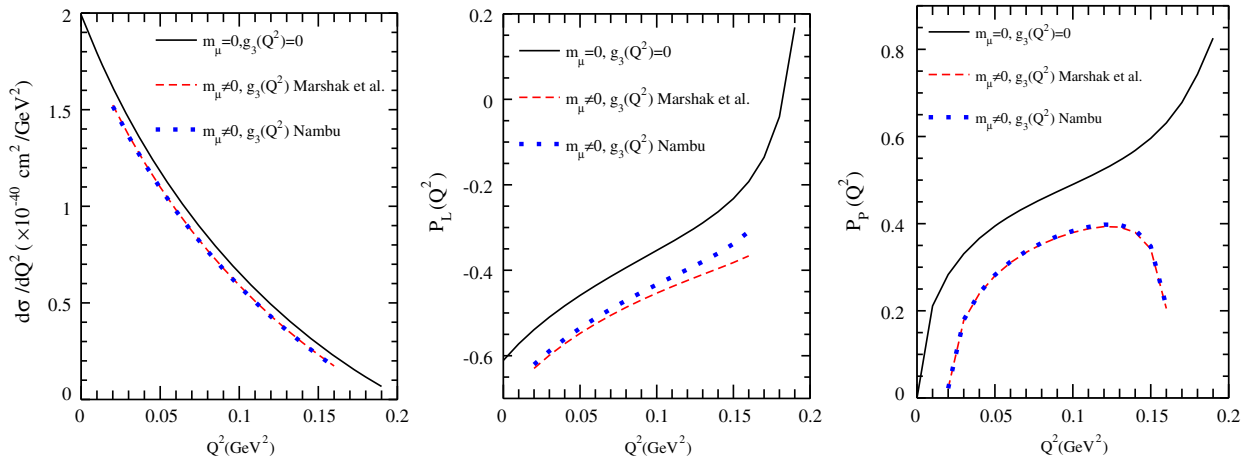

FIG. 11. Here are $\frac{d\sigma}{dQ^2}$, $P_L(Q^2)$, and $P_P(Q^2)$ vs Q^2 for the process $\bar{\nu}_\mu n \to \mu^+\Sigma^-$ at $E_{\bar{\nu}_\mu} = 0.5$ GeV. Lines and points have the same meaning as in Fig. 8.

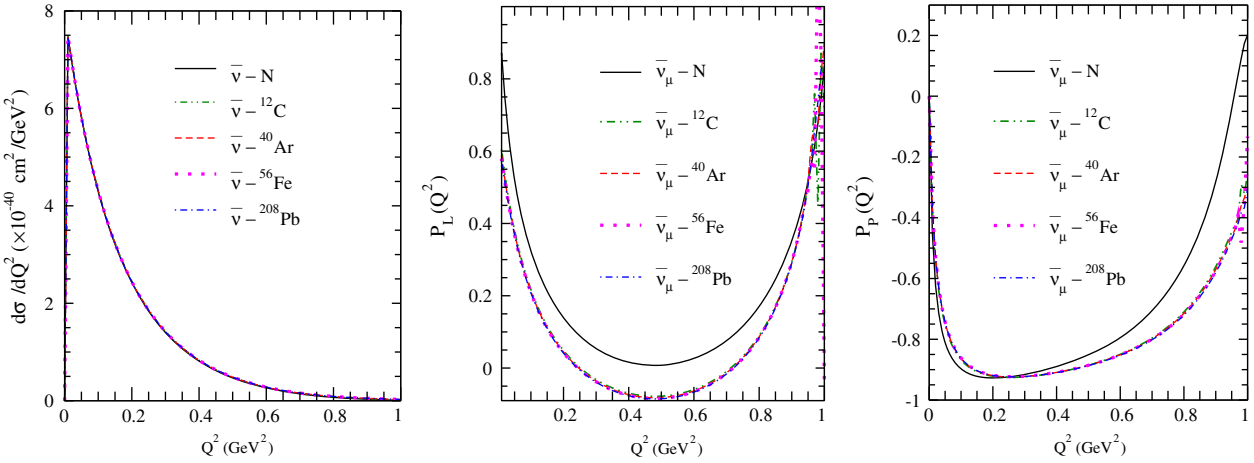

FIG. 12. Here are $\frac{d\sigma}{dQ^2}$, $P_L(Q^2)$, and $P_P(Q^2)$ vs Q^2 for the process $\bar{\nu}_\mu p \to \mu^+ \Lambda$ at $E_{\bar{\nu}_\mu} = 1$ GeV for free nucleon (solid line) and different nuclei per interacting particle viz. ^{12}C (dashed-double dotted), ^{40}Ar (dashed line), ^{56}Fe (dotted line), and ^{208}Pb (dashed-dotted line) with $m_\mu \neq 0$, $M_A = 1.026$ GeV. We have used $f_1^{p\Lambda}(Q^2)$, $f_2^{p\Lambda}(Q^2)$, and $g_1^{p\Lambda}(Q^2)$ from Table I and BBBA05 parametrization for nucleon form factors.

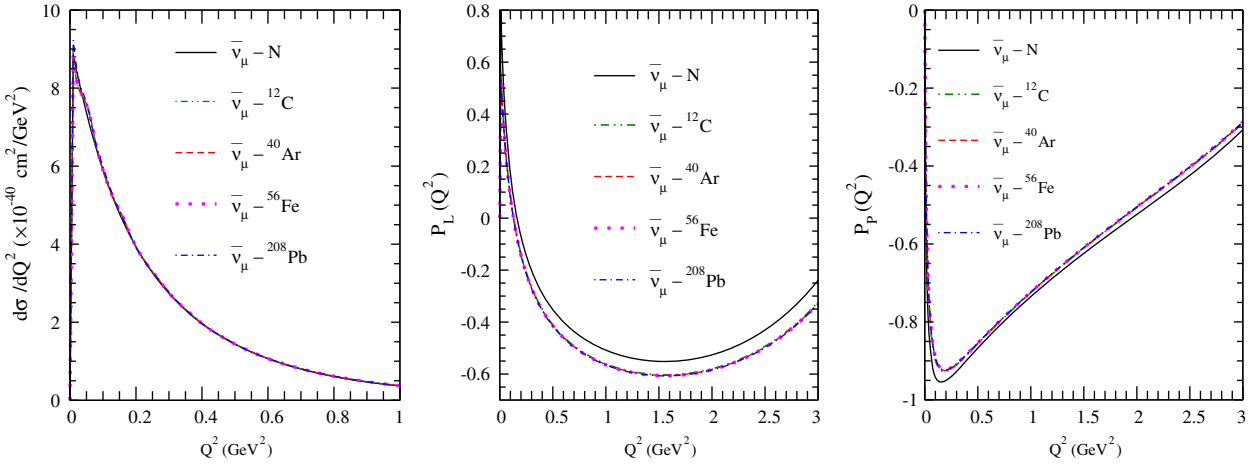

FIG. 13. Here are $\frac{d\sigma}{dQ^2}$, $P_L(Q^2)$, and $P_P(Q^2)$ vs Q^2 for the process $\bar{\nu}_\mu p \to \mu^+ \Lambda$ at $E_{\bar{\nu}_\mu} = 3$ GeV. Lines and points have the same meaning as Fig. 12.

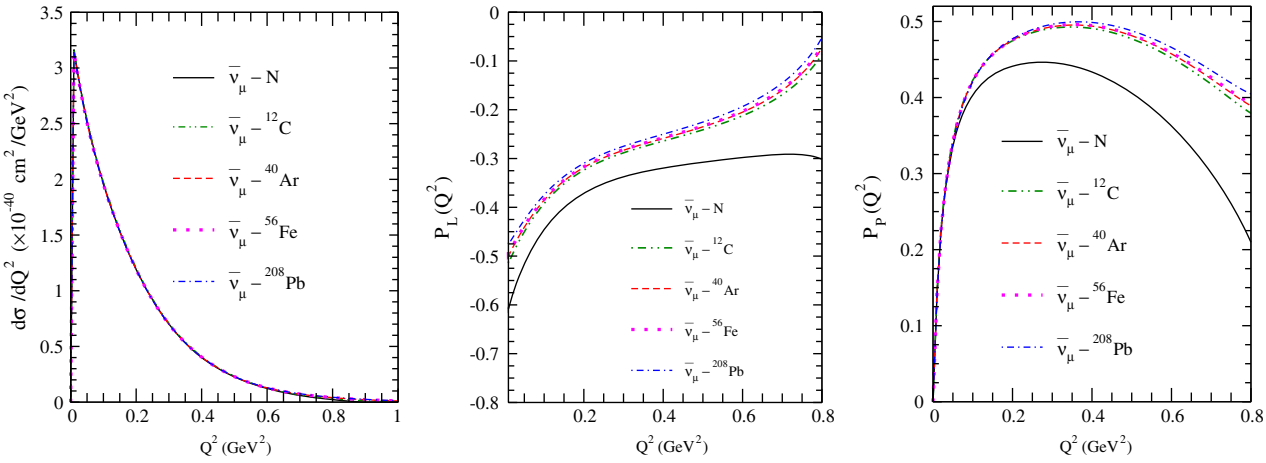

FIG. 14. Here are $\frac{d\sigma}{dQ^2}$, $P_L(Q^2)$, and $P_P(Q^2)$ vs Q^2 for the process $\bar{\nu}_\mu n \to \mu^+ \Sigma^-$ at $E_{\bar{\nu}_\mu} = 1$ GeV. Lines and points have the same meaning as Fig. 12.

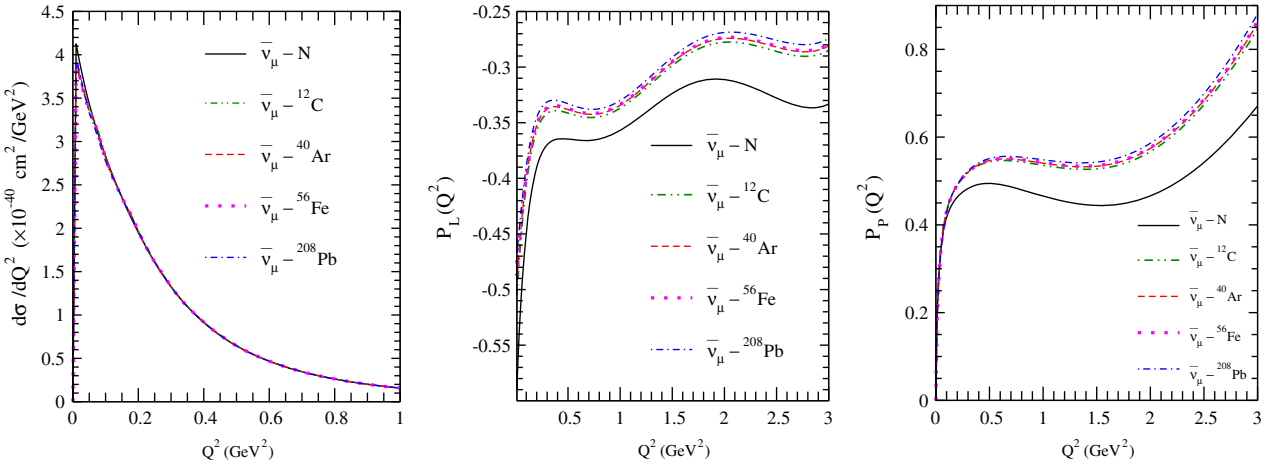

FIG. 15. Here are $\frac{d\sigma}{dQ^2}$, $P_L(Q^2)$, and $P_P(Q^2)$ vs Q^2 for the process $\bar{\nu}_\mu n \to \mu^+\Sigma^-$ at $E_{\bar{\nu}_\mu} = 3$ GeV. Lines and points have the same meaning as Fig. 12.

perpendicular ($P_P(Q^2)$) components of Λ and Σ polarization at $E_{\bar{\nu}_\mu} = 1$ and 3 GeV for various nuclei like ^{12}C, ^{40}Ar, ^{56}Fe, and ^{208}Pb using Eqs. (16), (31), and (32). The results are compared with the results for the free nucleon case. We find that at $E_{\bar{\nu}_\mu} = 1$ GeV the differential cross section $\frac{d\sigma}{dQ^2}$ hardly changes with the inclusion of nuclear medium effects. This is in contrast to the quasielastic reaction $\nu_l(\bar{\nu}_l) + n(p) \to l^-(l^+) + p(n)$. This is due to the lack of any Pauli blocking of the momentum of the final hyperon which has its own Fermi sea. The polarization observables $P_L(Q^2)$ and $P_P(Q^2)$ show some dependence on nuclear medium effects. The nature of this dependence is different for $P_L(Q^2)$ and $P_P(Q^2)$ as well as it is different for Λ and Σ hyperons. For example, in the case of $\bar{\nu}_\mu p \to \mu^+\Lambda$, the result for $P_L(Q^2)$ at low Q^2 is hardly affected by nuclear medium effects; however, with the increase in Q^2, the effect of nuclear medium increases. The effect becomes maximum for $Q^2 \sim 0.5$ GeV^2 and then decreases with further increase in Q^2. While in the case of $P_P(Q^2)$, the effect is smaller as compared to $P_L(Q^2)$, i.e., almost negligible for $Q^2 < 0.4$ GeV^2 and a slight increase for $Q^2 > 0.4$ GeV^2.

For $\bar{\nu}_\mu n \to \mu^+\Sigma^-$, the difference in the results obtained for nucleon and nuclear targets increases with the increase in Q^2, both for $P_L(Q^2)$ and $P_P(Q^2)$. Furthermore, we find that there is very little nuclear mass number (A) dependence of nuclear medium effects. Moreover, the nuclear effect becomes smaller with the increase in antineutrino energy.

C. Flux averaged differential cross section and polarization components

Currently, there are some neutrino experiments which are making measurements on neutrino-nucleus cross sections [31,33,58]. The LArTPC detector proposed for MicroBooNE [30], ArgoNeut [31], LAr1-ND, ICARUS-T600 [34], and DUNE [32] may be able to measure the tracks corresponding to nucleon and pion coming from Λ decay. A measurement of the asymmetry in the angular distribution of pions will give information about the hyperon (Λ, Σ^-) polarization. For the purpose of analyzing these experiments, we have convoluted $\frac{d\sigma}{dQ^2}$ and $P_{L,P}(Q^2)$ distributions over the flux $\Phi(E_{\bar{\nu}_\mu})$ available for different experiments using the expression given by

$$\langle F(Q^2)\rangle = \frac{\int_{E_{\rm th}}^{E_{\rm max}} F(Q^2, E_{\bar{\nu}_\mu})\Phi(E_{\bar{\nu}_\mu})dE_{\bar{\nu}_\mu}}{\int_{E_{\rm min}}^{E_{\rm max}} \Phi(E_{\bar{\nu}_\mu})dE_{\bar{\nu}_\mu}}, \qquad (37)$$

where the function $F(Q^2, E_{\bar{\nu}_\mu})$ represents $\frac{d\sigma}{dQ^2}(Q^2, E_{\bar{\nu}_\mu})$, $P_L(Q^2, E_{\bar{\nu}_\mu})$, and $P_P(Q^2, E_{\bar{\nu}_\mu})$ given in Eqs. (16), (31), and (32), respectively. Here, E_{th}, $E_{\rm min}$, and $E_{\rm max}$ are the threshold energy and the minimum and maximum energies of the antineutrino fluxes corresponding to these experiments, respectively. In Figs. 16 and 17, we have shown the flux averaged $\langle\frac{d\sigma}{dQ^2}\rangle$, $\langle P_L(Q^2)\rangle$, and $\langle P_P(Q^2)\rangle$ for reactions $\bar{\nu}_\mu p \to \mu^+\Lambda$ and $\bar{\nu}_\mu n \to \mu^+\Sigma^-$, respectively, corresponding to the MicroBooNE [30] antineutrino experiment in ^{40}Ar using $M_A = 1.026$ GeV and $g_3^{NY}(Q^2) \neq 0$.

We have also shown in Figs. 18 and 19 the flux averaged results of $\langle\frac{d\sigma}{dQ^2}\rangle$, $\langle P_L(Q^2)\rangle$, and $\langle P_P(Q^2)\rangle$ for reactions $\bar{\nu}_\mu p \to \mu^+\Lambda$ and $\bar{\nu}_\mu n \to \mu^+\Sigma^-$, respectively, for the ^{12}C target corresponding to the T2K [58] antineutrino spectrum. Similar results are presented for these reactions corresponding to the MINERνA [33] experiment in the ^{208}Pb target for the antineutrino beam with an average energy of 3.6 GeV in Figs. 20 and 21. It may be observed from these figures that polarization measurements on $\bar{\nu}_\mu p \to \mu^+\Lambda$ and $\bar{\nu}_\mu n \to \mu^+\Sigma^-$ in all these experiments will

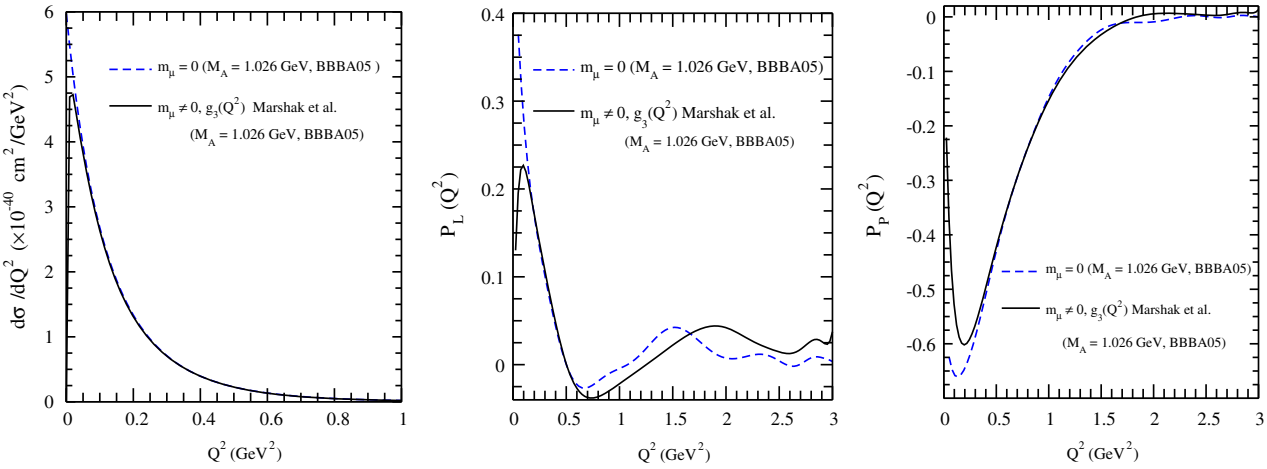

FIG. 16. Here are $\frac{d\sigma}{dQ^2}$, $P_L(Q^2)$, and $P_P(Q^2)$ vs Q^2 for the process $\bar{\nu}_\mu p \to \mu^+\Lambda$ (^{40}Ar target) averaged over the MicroBooNE [30] spectrum, using $f_1^{p\Lambda}(Q^2), f_2^{p\Lambda}(Q^2), g_1^{p\Lambda}(Q^2)$ from Table I and the BBBA05 parametrization [35] for the nucleon form factors with $m_\mu = 0$ and $M_A = 1.026$ GeV (dashed line), and $m_\mu \neq 0$, $M_A = 1.026$ GeV with $g_3^{p\Lambda}(Q^2)$ from Marshak *et al.* [17] (solid line).

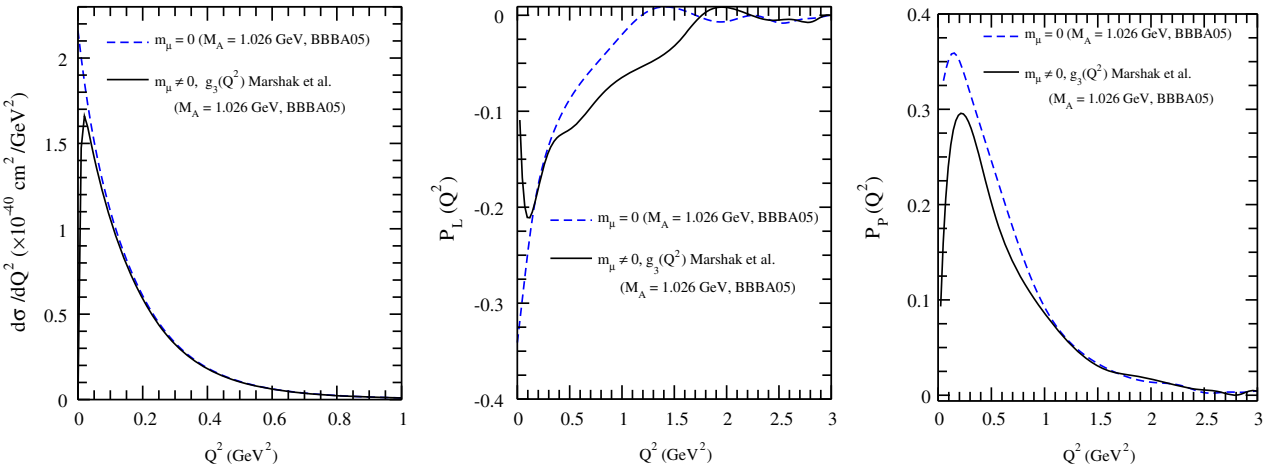

FIG. 17. Here are $\frac{d\sigma}{dQ^2}$, $P_L(Q^2)$, and $P_P(Q^2)$ vs Q^2 for the process $\bar{\nu}_\mu n \to \mu^+\Sigma^-$ (^{40}Ar target) averaged over the MicroBooNE [30] spectrum. Lines and points have the same meaning as in Fig. 16.

enable us to independently determine the value of the axial vector form factor in the strangeness sector.

Moreover, at lower $\bar{\nu}_\mu$ energies relevant to MicroBooNE [30] and T2K [58] experiments, it is also possible to determine the pseudoscalar from factors and test the hypothesis of PCAC in the strangeness sector.

D. Energy dependence of total cross section and average polarizations

We have calculated the total cross section $\sigma(E_{\bar{\nu}_\mu})$ as a function of energy, given as

$$\sigma(E_{\bar{\nu}_\mu}) = \int_{Q^2_{\min}}^{Q^2_{\max}} \frac{d\sigma}{dQ^2}(Q^2, E_{\bar{\nu}_\mu}) dQ^2, \tag{38}$$

for $\bar{\nu}_\mu p \to \mu^+\Lambda$ and $\bar{\nu}_\mu p \to \mu^+\Sigma^0$ reactions. We show the results for $\sigma(E_{\bar{\nu}_\mu})$ in Fig. 22, where a comparison is made with available experimental results from CERN [4–6], BNL [7], FNAL [8,9], and Serpukhov [10] experiments. A reasonable agreement with the experimental results can be seen. We also show in Fig. 23 the energy dependence of averaged polarization components $P_L(E_{\bar{\nu}_\mu})$ and $P_P(E_{\bar{\nu}_\mu})$ for completeness which are defined as [67]

$$\langle P_{L,P}(E_{\bar{\nu}_\mu})\rangle = \frac{\int_{Q^2_{\min}}^{Q^2_{\max}} P_{L,P}(Q^2, E_{\bar{\nu}_\mu}) \frac{d\sigma}{dQ^2} dQ^2}{\int_{Q^2_{\min}}^{Q^2_{\max}} \frac{d\sigma}{dQ^2} dQ^2}, \tag{39}$$

for the processes $\bar{\nu}_\mu p \to \mu^+\Lambda$ and $\bar{\nu}_\mu n \to \mu^+\Sigma^-$. It may be observed from Fig. 23 that for the process $\bar{\nu}_\mu p \to \mu^+\Lambda$, the

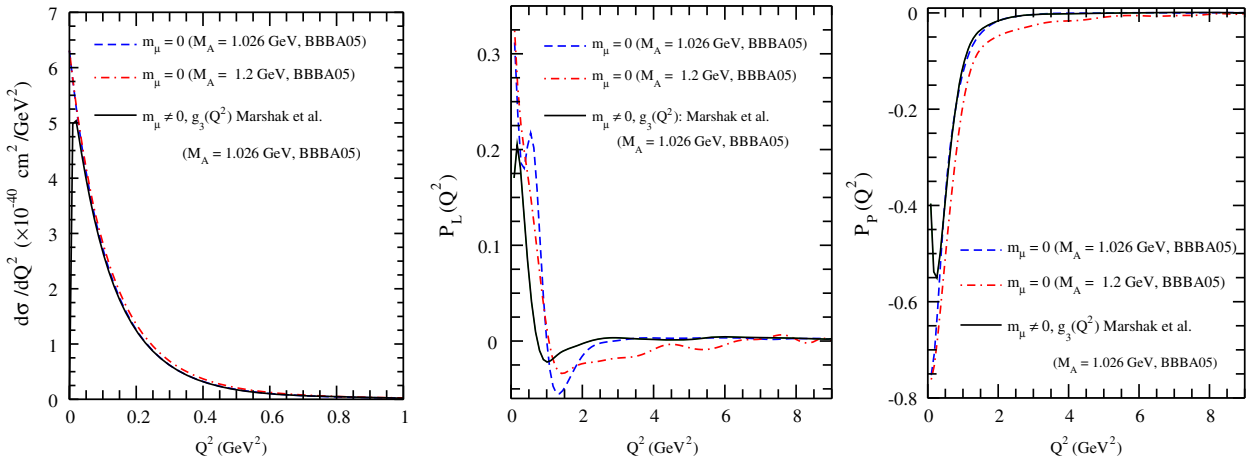

FIG. 18. Here are $\frac{d\sigma}{dQ^2}$, $P_L(Q^2)$, and $P_P(Q^2)$ vs Q^2 for the process $\bar{\nu}_\mu p \to \mu^+ \Lambda$ (^{12}C target) averaged over the T2K [58] spectrum, using $f_1^{p\Lambda}(Q^2), f_2^{p\Lambda}(Q^2), g_1^{p\Lambda}(Q^2)$ from Table I and the BBBA05 parametrization [35] for the nucleon form factors with $m_\mu = 0$ and $M_A = 1.026$ GeV (dashed line), $m_\mu = 0$ and $M_A = 1.2$ GeV (dashed–dotted line) and $m_\mu \neq 0$, $M_A = 1.026$ GeV with $g_3^{p\Lambda}(Q^2)$ from Marshak *et al.* [17] (solid line).

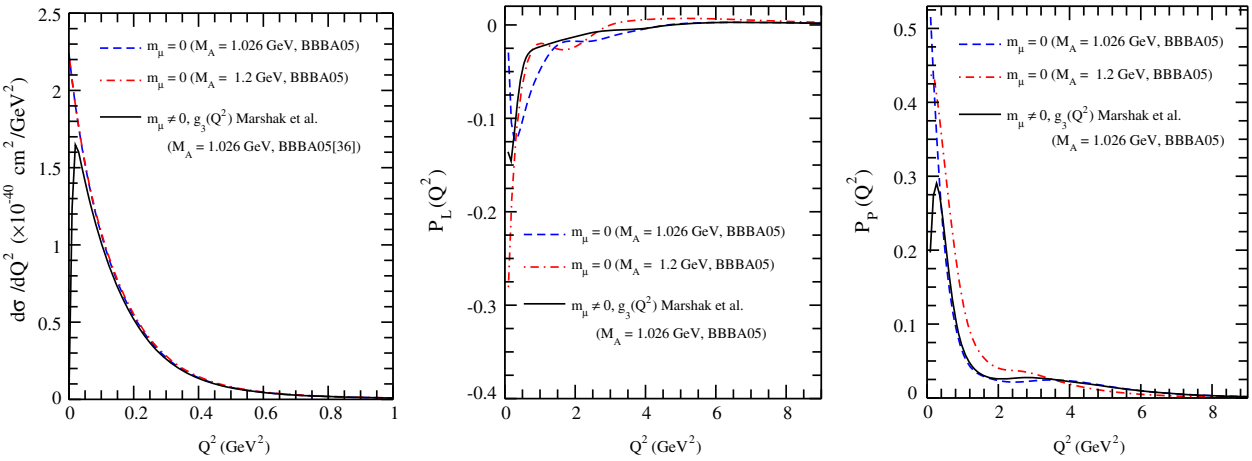

FIG. 19. Here are $\frac{d\sigma}{dQ^2}$, $P_L(Q^2)$, and $P_P(Q^2)$ vs Q^2 for the process $\bar{\nu}_\mu n \to \mu^+ \Sigma^-$ (^{12}C target) averaged over the T2K [58] spectrum. Lines and points have the same meaning as in Fig. 18.

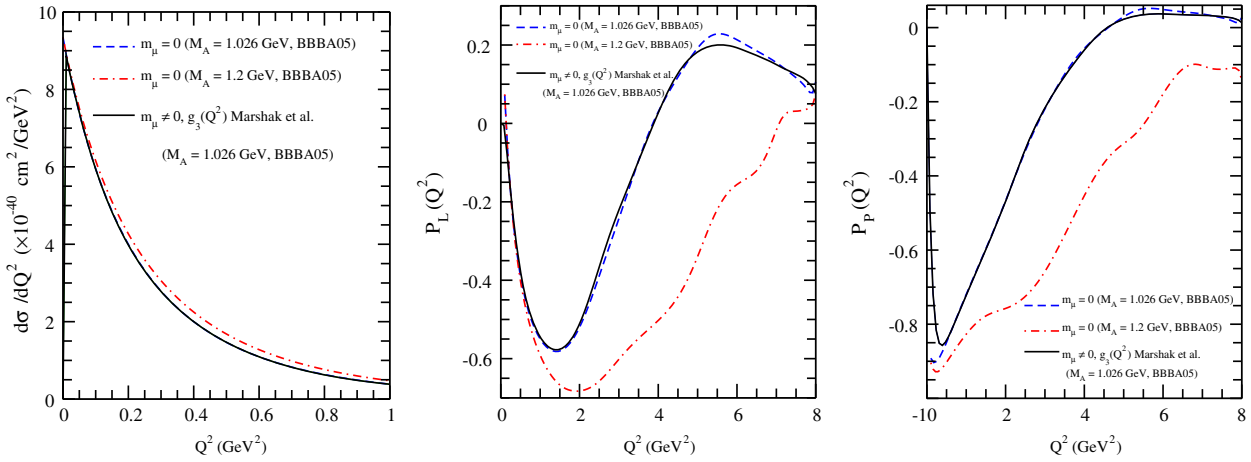

FIG. 20. Here are $\frac{d\sigma}{dQ^2}$, $P_L(Q^2)$, and $P_P(Q^2)$ vs Q^2 for the process $\bar{\nu}_\mu p \to \mu^+ \Lambda$ (^{208}Pb target) averaged over MINERνA [33] spectrum. Lines and points have the same meaning as in Fig. 18.

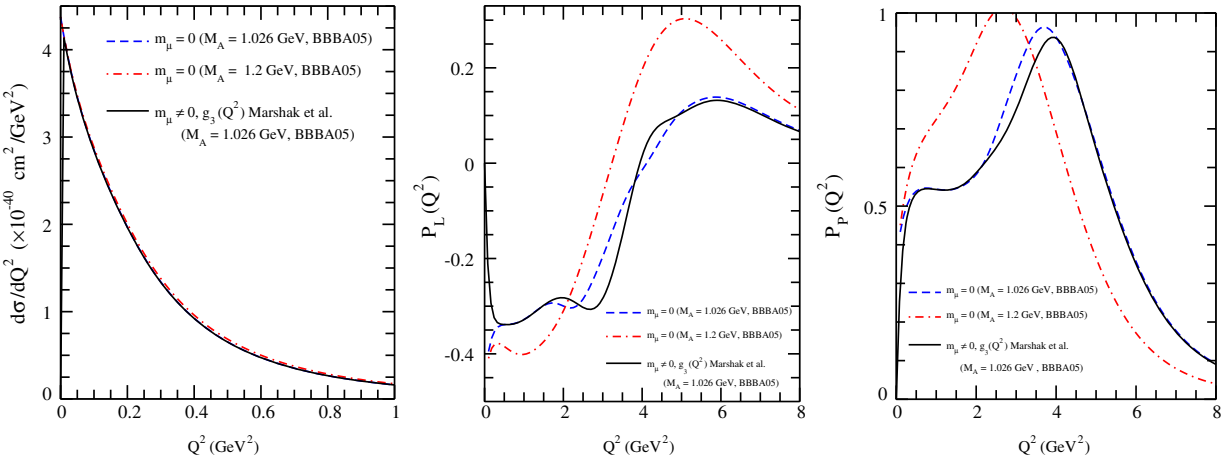

FIG. 21. Here are $\frac{d\sigma}{dQ^2}$, $P_L(Q^2)$, and $P_P(Q^2)$ vs Q^2 for the process $\bar{\nu}_\mu n \to \mu^+\Sigma^-$ (^{208}Pb target) averaged over the MINERνA [33] spectrum. Lines and points have the same meaning as in Fig. 18.

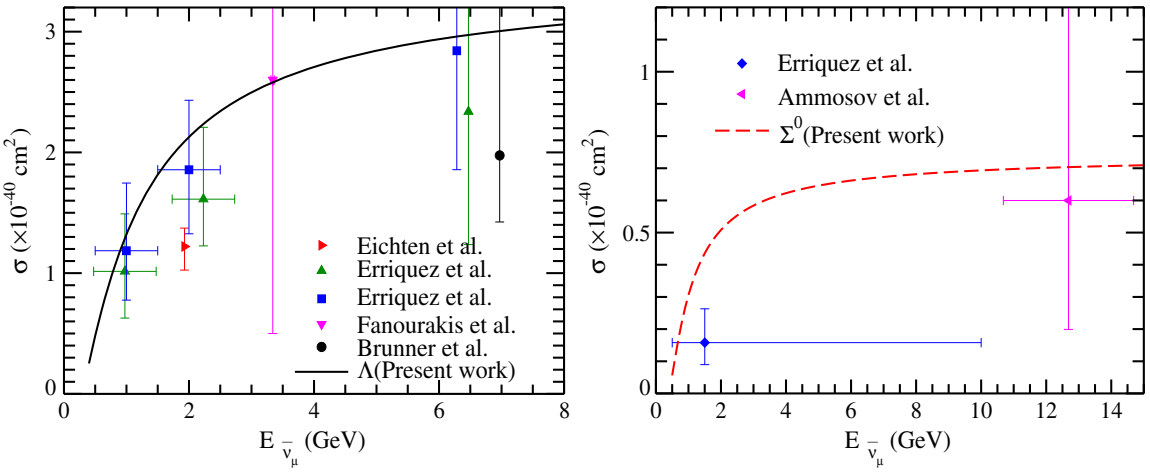

FIG. 22. Theoretical curves for total cross section (σ) vs $E_{\bar{\nu}_\mu}$ corresponding to the processes $\bar{\nu}_\mu p \to \mu^+\Lambda$ (solid line) in the left panel and $\bar{\nu}_\mu p \to \mu^+\Sigma^0$ (dashed line) in the right panel using $f_1^{NY}(Q^2), f_2^{NY}(Q^2), g_1^{NY}(Q^2)$ from Table I, $g_3^{NY}(Q^2)$ from Marshak *et al.* [17] given in Eq. (8) with $M_A = 1.026$ GeV. Experimental results for the process $\bar{\nu}_\mu p \to \mu^+\Lambda$ (triangle right [5], triangle up [4], square [6], triangle down ($\sigma = 2.6^{+5.9}_{-2.1} \times 10^{-40}$ cm^2) [7], circle [10]) and for the process $\bar{\nu}_\mu p \to \mu^+\Sigma^0$ (diamond [4]) are shown with error bars.

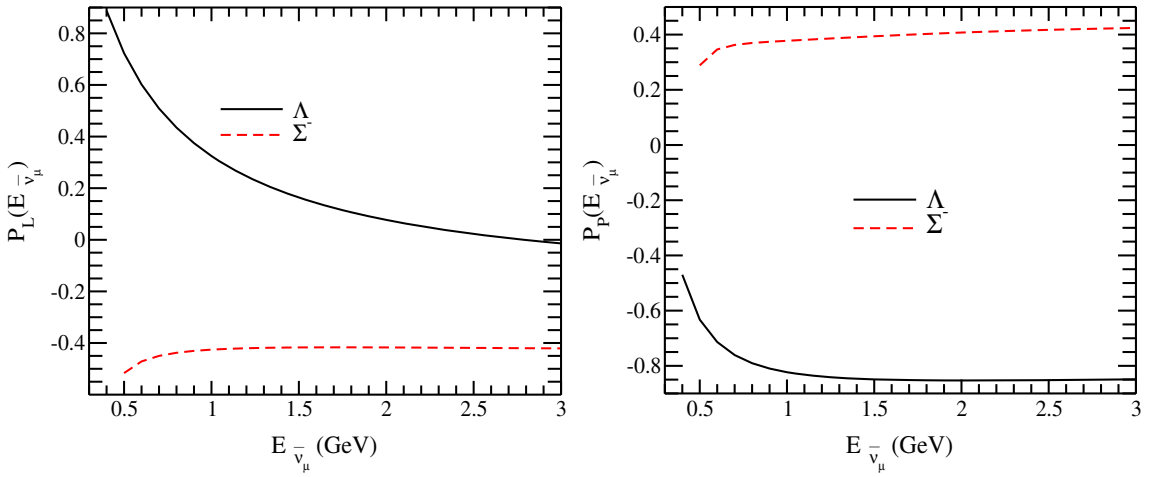

FIG. 23. Polarization components $P_L(E_{\bar{\nu}_\mu})$ and $P_P(E_{\bar{\nu}_\mu})$ vs $E_{\bar{\nu}_\mu}$ using Eq. (39) for the processes $\bar{\nu}_\mu p \to \mu^+\Lambda$ (solid line) and $\bar{\nu}_\mu n \to \mu^+\Sigma^-$ (dashed line) using $f_1^{NY}(Q^2), f_2^{NY}(Q^2), g_1^{NY}(Q^2)$ from Table I and $g_3^{NY}(Q^2)$ from Marshak *et al.* [17] with $M_A = 1.026$ GeV.

TABLE II. Flux averaged cross section $\langle\sigma\rangle$ (using Eq. (40), longitudinal $\langle P_L\rangle$, and perpendicular $\langle P_P\rangle$ components of polarization [using Eq. (41)] are given for the process $\bar{\nu}_\mu p \to \mu^+\Lambda$.

	$\langle P_L\rangle$	$\langle P_P\rangle$[a]	$\langle\sigma\rangle \times (10^{-40}$ cm$^2)$
Experiments			
Erriquez *et al.* [6]	-0.06 ± 0.44	1.05 ± 0.30	2.07 ± 0.75
Erriquez *et al.* [4]	...	...	1.40 ± 0.41 (Propane)
Eichten *et al.* [5]	...	...	$1.3 \pm^{0.9}_{0.7}$ (Freon)
Theory			
Present work ($M_A = 0.84$ GeV)	0.10	−0.75	2.00
($M_A = 1.026$ GeV)	0.05	−0.85	2.15
($M_A = 1.2$ GeV)	0.03	−0.89	2.31
Erriquez *et al.* [6] ($M_A = 0.84$ GeV)	0.14	0.73	2.07

[a]One may note that, for present work, we have considered the sign convention for perpendicular polarization which is opposite to that of used by Erriquez *et al.* [6].

polarization components $P_L(E_{\bar{\nu}_\mu})$ and $P_P(E_{\bar{\nu}_\mu})$ decrease with the increase in energy, while for the process $\bar{\nu}_\mu n \to \mu^+\Sigma^-$ these polarization components increase with the energy initially and then become almost constant.

E. Total cross section and polarizations

We have integrated the differential cross section $\frac{d\sigma}{dQ^2}$ and polarization observables $P_L(Q^2)$ and $P_P(Q^2)$ over $E_{\bar{\nu}_\mu}$ and Q^2 distributions to obtain the total cross section $\langle\sigma\rangle$ defined as

$$\langle\sigma\rangle = \frac{\int_{E_{th}}^{E_{\max}} \int_{Q^2_{\min}}^{Q^2_{\max}} \frac{d\sigma}{dQ^2} dQ^2 \Phi(E_{\bar{\nu}_\mu}) dE_{\bar{\nu}_\mu}}{\int_{E_{\min}}^{E_{\max}} \Phi(E_{\bar{\nu}_\mu}) dE_{\bar{\nu}_\mu}} \tag{40}$$

and components of hyperon polarization $\langle P_{L,P}\rangle$ defined as

$$\langle P_{L,P}\rangle = \frac{1}{\langle\sigma\rangle} \int_{E_{th}}^{E_{\max}} \int_{Q^2_{\min}}^{Q^2_{\max}} P_{L,P}(Q^2, E_{\bar{\nu}_\mu}) \times \frac{d\sigma}{dQ^2} dQ^2 \Phi(E_{\bar{\nu}_\mu}) dE_{\bar{\nu}_\mu}. \tag{41}$$

In order to compare with the experimental results of the CERN experiment [6], we have performed the numerical calculations for the flux averaged cross section $\langle\sigma\rangle$, longitudinal $\langle P_L\rangle$, and perpendicular $\langle P_P\rangle$ polarization components relevant for the antineutrino flux of SPS antineutrino beam of Gargamelle experiment at CERN [68] and present our results in Table II. The results are compared with the available experimental results from the CERN [4–6] experiment and the theoretical results quoted by Erriquez *et al.* [6]. For reference we also show in Table III, our results for $\langle\sigma\rangle$, $\langle P_L\rangle$, and $\langle P_P\rangle$ relevant for MicroBooNE [30], MINERνA [33], and T2K [58] experiments, which may be useful in the interpretation of the results from these experiments, whenever they become available.

TABLE III. Total cross section using Eq. (40) and longitudinal and perpendicular components of polarization using Eq. (41) are integrated over various fluxes for the $\bar{\nu}_\mu(k) + N(p) \to \mu^+(k') + Y(p')$ process using $f_1^{NY}(Q^2), f_2^{NY}(Q^2), g_1^{NY}(Q^2)$ from Table I and $g_3^{NY}(Q^2)$ from Eq. (8) with $m_\mu \neq 0$ and $M_A = 1.026$ GeV.

	$\langle\sigma\rangle \times 10^{-40}$ cm^2		$\langle P_L\rangle$		$\langle P_P\rangle$	
Spectrum	Σ^-	Λ	Σ^-	Λ	Σ^-	Λ
MicroBooNE [30]	0.31	0.76	−0.43	0.39	0.37	−0.78
MINERνA [33]	1.17	2.5	−0.42	−0.03	0.43	−0.85
T2K [58]	0.27	0.74	−0.44	0.43	0.37	−0.75

IV. SUMMARY AND CONCLUSIONS

We have in this work studied the differential cross section $\frac{d\sigma}{dQ^2}$ as well as longitudinal ($P_L(Q^2)$) and perpendicular ($P_P(Q^2)$) components of polarization of Λ and Σ hyperons produced in the quasielastic reactions of antineutrinos on free and bound nucleons. The effect of the nuclear medium arising due to Fermi motion and Pauli blocking for the initial nucleon have been included. The transition form factors for the nucleon-hyperon transition have been obtained using Cabibbo theory assuming SU(3) invariance and the absence of second class currents. The sensitivity of Q^2 dependence on $\frac{d\sigma}{dQ^2}$, $P_L(Q^2)$, and $P_P(Q^2)$ due to the variation in M_A has been studied. The possibility of determining the pseudoscalar form factor in the $|\Delta S| = 1$ sector has also been explored. The theoretical results have been compared with the available experimental results on the energy dependence of the total cross sections from CERN [4–6] and other experiments performed at BNL [7], FNAL [8,9], and Serpukhov [10]. A comparison of our theoretical results with the experimental results on the flux averaged total cross section and averaged polarization components for the CERN [6] experiment has also been made. Predictions for the flux averaged cross section and polarization components

have been made for the future experiments being done on nuclear targets with antineutrino beams at MicroBooNE [30], MINERνA [33], and T2K [58].

To summarize our results we find the following:

(1) The theoretical results for the total cross section as a function of energy, i.e., $\sigma(E_{\bar{\nu}_\mu})$ is found to be in satisfactory agreement with the earlier experimental results available from CERN, BNL, and Serpukhov laboratories with an axial mass of $M_A = 1.026$ GeV, the world average value obtained from $\Delta S = 0$ experiments.

(2) The longitudinal and perpendicular components of polarization $P_L(Q^2)$ and $P_P(Q^2)$ are sensitive to the value of axial dipole mass M_A. Therefore, it is possible to determine the value of M_A independent of the cross section measurements for the single hyperon production.

(3) The Q^2 dependence of the cross section $\frac{d\sigma}{dQ^2}$ and polarization components $P_{L,P}(Q^2)$ are found to be sensitive to the neutron charge form factor in the case of $\bar{\nu}_\mu n \to \mu^+ \Sigma^-$ process, especially for $Q^2 > 0.2$ GeV^2.

(4) At lower antineutrino energies $E_{\bar{\nu}_\mu} \sim 0.5$ GeV, the differential cross section $\frac{d\sigma}{dQ^2}$ and the polarization components $P_{L,P}(Q^2)$ are sensitive to the value of pseudoscalar form factor. It should be possible to test PCAC and the GT relation in the strangeness sector, from the quasielastic production of hyperons at lower energies relevant to MicroBooNE and T2K experiments. At antineutrino energies $E_{\bar{\nu}_\mu} \geq 1$ GeV, the differential cross section $\frac{d\sigma}{dQ^2}$ and the polarization components are not found to be sensitive to the pseudoscalar form factor.

(5) The effect of nuclear medium on $\frac{d\sigma}{dQ^2}$, $P_L(Q^2)$, and $P_P(Q^2)$ arising due to Fermi motion and Pauli blocking of initial nucleon are studied quantitatively. They are found to be quite small and negligible for $\frac{d\sigma}{dQ^2}$. However, these effects are found to be non-negligible but small for $P_L(Q^2)$ and $P_P(Q^2)$ and show no appreciable dependence on the nucleon number A.

It should be emphasized that we have assumed in our present work the absence of second class currents. If such currents are present, the results are expected to get modified. Moreover, the presence of second class currents will also give rise to T-violating effects in quasielastic hyperon production induced by antineutrinos. This work is in progress and will be reported in the future.

ACKNOWLEDGMENTS

M. S. A. is thankful to the Department of Science and Technology(DST), Government of India, for providing financial assistance under Grant No. SR/S2/HEP-18/2012.

APPENDIX: EXPRESSIONS FOR COEFFICIENTS OF CROSS SECTION AND POLARIZATION OBSERVABLES

The expressions for $\mathcal{N}(Q^2, E_{\bar{\nu}_\mu})$, $\mathcal{A}(Q^2, E_{\bar{\nu}_\mu})$, and $\mathcal{B}(Q^2, E_{\bar{\nu}_\mu})$ are given as

$$
\begin{aligned}
\mathcal{N}(Q^2, E_{\bar{\nu}_\mu}) = {} & f_1^2(2E_{\bar{\nu}_\mu}(\vec{k}\cdot\vec{k}' + 2m_N E_\mu - m_\mu^2) - 2\vec{k}\cdot\vec{k}'(m_Y + E_\mu)) \\
& + \frac{f_2^2}{(m_N + m_Y)^2}(4(\vec{k}\cdot\vec{k}')^2(m_Y + E_\mu - E_{\bar{\nu}_\mu}) + \vec{k}\cdot\vec{k}'(m_N(4(E_\mu^2 + E_{\bar{\nu}_\mu}^2) - m_\mu^2) \\
& - 3m_\mu^2(m_Y + E_\mu - E_{\bar{\nu}_\mu})) - 4m_N m_\mu^2 E_{\bar{\nu}_\mu}^2) \\
& + g_1^2(2(\vec{k}\cdot\vec{k}'(m_Y - E_\mu + E_{\bar{\nu}_\mu}) - E_{\bar{\nu}_\mu}(m_\mu^2 - 2m_N E_\mu))) \\
& + g_3^2((\vec{k}\cdot\vec{k}')^2 m_\mu^2(m_N - m_Y - E_\mu + E_{\bar{\nu}_\mu})) \\
& + \frac{f_1 f_2}{m_N + m_Y}(8(\vec{k}\cdot\vec{k}')^2 + \vec{k}\cdot\vec{k}'(4(m_N - m_Y)(E_\mu - E_{\bar{\nu}_\mu}) - 6m_\mu^2) \\
& + 2m_\mu^2 E_{\bar{\nu}_\mu}(m_N - m_Y)) \\
& + f_1 g_1(-4(\vec{k}\cdot\vec{k}'(E_\mu + E_{\bar{\nu}_\mu}) - m_\mu^2 E_{\bar{\nu}_\mu})) \\
& + \frac{f_2 g_1}{m_N + m_Y}(-4(m_N + m_Y)(\vec{k}\cdot\vec{k}'(E_\mu + E_{\bar{\nu}_\mu}) - m_\mu^2 E_{\bar{\nu}_\mu})) \\
& + g_1 g_3(-2m_\mu^2(\vec{k}\cdot\vec{k}' + E_{\bar{\nu}_\mu}(m_Y - m_N))) \qquad \text{(A1)}
\end{aligned}
$$

$$\begin{aligned}\mathcal{A}(Q^2,E_{\bar{\nu}_\mu}) &= f_1^2(-2\vec{k}\cdot\vec{k}' - (m_N-m_Y)(E_\mu - E_{\bar{\nu}_\mu}) + m_\mu^2)\\ &+\frac{f_2^2}{(m_N+m_Y)^2}((2\vec{k}\cdot\vec{k}' - m_\mu^2)(2\vec{k}\cdot\vec{k}' + (m_N-m_Y)(E_\mu - E_{\bar{\nu}_\mu}) - m_\mu^2))\\ &+g_1^2(2\vec{k}\cdot\vec{k}' + (m_N+m_Y)(E_\mu - E_{\bar{\nu}_\mu}) - m_\mu^2) + \frac{f_1 f_2}{m_N+m_Y}(-2(2\vec{k}\cdot\vec{k}'(m_Y + E_\mu - E_{\bar{\nu}_\mu}) + m_N(E_\mu - E_{\bar{\nu}_\mu})^2\\ &+m_\mu^2(-(m_Y + E_\mu - E_{\bar{\nu}_\mu}))))+f_1 g_1(2m_Y(E_\mu + E_{\bar{\nu}_\mu})) + f_1 g_3(m_\mu^2(-m_N + m_Y + E_\mu - E_{\bar{\nu}_\mu}))\\ &+\frac{f_2 g_1}{m_N+m_Y}(-4\vec{k}\cdot\vec{k}'(E_\mu + E_{\bar{\nu}_\mu}) + m_N(m_\mu^2 - 2E_\mu^2 + 2E_{\bar{\nu}_\mu}^2) + m_\mu^2(m_Y + E_\mu + 3E_{\bar{\nu}_\mu}))\times\\ &+\frac{f_2 g_3}{m_N+m_Y}(m_\mu^2(-2\vec{k}\cdot\vec{k}' - (m_N-m_Y)(E_\mu - E_{\bar{\nu}_\mu}) + m_\mu^2)),\end{aligned} \tag{A2}$$

$$\begin{aligned}\mathcal{B}(Q^2,E_{\bar{\nu}_\mu}) &= f_1^2((E_\mu + E_{\bar{\nu}_\mu})(2\vec{k}\cdot\vec{k}' + m_Y(m_Y - m_N)) + m_\mu^2(m_Y - 2E_{\bar{\nu}_\mu}))\\ &+\frac{f_2^2}{(m_N+m_Y)^2}(4(\vec{k}\cdot\vec{k}')^2(E_\mu + E_{\bar{\nu}_\mu}) + 2\vec{k}\cdot\vec{k}'((E_\mu + E_{\bar{\nu}_\mu})(m_N(m_Y + 2E_\mu - 2E_{\bar{\nu}_\mu})\\ &+m_Y^2) - m_\mu^2(m_Y + E_\mu + 3E_{\bar{\nu}_\mu})) + m_\mu^2(-m_N(m_Y(E_\mu + E_{\bar{\nu}_\mu}) + 4E_{\bar{\nu}_\mu}(E_\mu - E_{\bar{\nu}_\mu}))\\ &+m_\mu^2(m_Y + 2E_{\bar{\nu}_\mu}) + m_Y^2(E_\mu - 3E_{\bar{\nu}_\mu})))+g_1^2((E_\mu + E_{\bar{\nu}_\mu})(2\vec{k}\cdot\vec{k}' + m_Y(m_N + m_Y)) - m_\mu^2(m_Y + 2E_{\bar{\nu}_\mu}))\\ &+\frac{f_1 f_2}{m_N+m_Y}(2(m_N(E_\mu + E_{\bar{\nu}_\mu})(2\vec{k}\cdot\vec{k}' + m_Y(E_{\bar{\nu}_\mu} - E_\mu)) + m_\mu^2(m_Y(m_Y + E_\mu)\times\\ &+E_{\bar{\nu}_\mu}(2m_N + m_Y))))+f_1 g_1(2E_\mu(2\vec{k}\cdot\vec{k}' + m_Y^2) - 2E_{\bar{\nu}_\mu}(2\vec{k}\cdot\vec{k}' + 4m_N E_\mu - 2m_\mu^2 + m_Y^2))\\ &+f_1 g_3(m_\mu^2(2\vec{k}\cdot\vec{k}' - m_N(m_Y + 2E_{\bar{\nu}_\mu}) + m_Y(m_Y + E_\mu - E_{\bar{\nu}_\mu})))\\ &+\frac{f_2 g_1}{m_N+m_Y}(-8(\vec{k}\cdot\vec{k}')^2 + \vec{k}\cdot\vec{k}'(6m_\mu^2 - 4(m_N E_\mu - m_N E_{\bar{\nu}_\mu} + m_Y^2))\\ &+m_N(m_\mu^2(m_Y - 2E_{\bar{\nu}_\mu}) - 2m_Y(E_\mu + E_{\bar{\nu}_\mu})^2) + m_\mu^2 m_Y(m_Y + E_\mu + 3E_{\bar{\nu}_\mu}))\\ &+\frac{f_2 g_3}{m_N+m_Y}(m_\mu^2((E_\mu + E_{\bar{\nu}_\mu})(2\vec{k}\cdot\vec{k}' + m_Y(m_Y - m_N)) + m_\mu^2(m_Y - 2E_{\bar{\nu}_\mu}))).\end{aligned} \tag{A3}$$

$$\begin{aligned}\alpha(Q^2,\vec{p}) = \frac{64}{m_Y}\Bigg[&f_1^2(k\cdot k'k\cdot p - m_N m_Y(k\cdot k' + k'\cdot p - m_\mu^2) + k\cdot k'k'\cdot p - k\cdot pm_\mu^2 + k'\cdot pm_Y^2)\\ &+\frac{f_2^2}{(m_N+m_Y)^2}(2k\cdot k'^2(k\cdot p + k'\cdot p + m_N m_Y) - k\cdot k'(2k\cdot p^2 + 3k\cdot pm_\mu^2 - 2k\cdot pm_Y^2 - 2k'\cdot p^2\\ &-2k'\cdot pm_N m_Y + k'\cdot pm_\mu^2 + 3m_N m_\mu^2 m_Y) + m_\mu^2(2k\cdot p^2 + k\cdot p(-2k'\cdot p + m_\mu^2 - 2m_Y^2)\\ &+m_Y(-k'\cdot pm_N + k'\cdot pm_Y + m_N m_\mu^2)))g_1^2(k\cdot k'(k\cdot p + k'\cdot p + m_N m_Y)\\ &-k\cdot pm_\mu^2 + m_Y(k'\cdot p(m_N + m_Y) - m_N m_\mu^2))\\ &\times\frac{f_1 f_2}{m_N+m_Y}(2(k\cdot k'm_N(k\cdot p + k'\cdot p) + m_Y(k\cdot p - k'\cdot p)(k\cdot k' + k'\cdot p - m_\mu^2)\\ &+m_N m_Y^2(m_\mu^2 - k\cdot k') - k\cdot pm_N m_\mu^2)) + f_1 g_1(2(k\cdot k'(k'\cdot p - k\cdot p) + k\cdot p(m_\mu^2 - 2k'\cdot p) + k'\cdot pm_Y^2))\\ &+f_1 g_3(m_\mu^2(k\cdot k'm_N - k\cdot p(m_N + m_Y) + m_Y(k'\cdot p + m_N m_Y - m_N)))\\ &\times\frac{f_2 g_1}{m_N+m_Y}(-4k\cdot k'^2 m_N + k\cdot k'(m_N(2k\cdot p - 2k'\cdot p + 3m_\mu^2) - 2m_Y(k\cdot p + k'\cdot p) - 2m_N m_Y^2)\\ &-m_\mu^2(k\cdot p(m_N - 3m_Y) - m_Y(k'\cdot p + m_N m_Y + m_N)) - 2k'\cdot pm_Y(k\cdot p + k'\cdot p))\\ &+\frac{f_2 g_3}{m_N+m_Y}(m_\mu^2(k\cdot k'k\cdot p - m_N m_Y(k\cdot k' + k'\cdot p - m_\mu^2) + k\cdot k'k'\cdot p - k\cdot pm_\mu^2 + k'\cdot pm_Y^2))\Bigg]\end{aligned} \tag{A4}$$

$$\beta(Q^2,\vec{p}) = \frac{64}{m_Y}\Big[f_1^2(k\cdot p(m_Y(m_N-m_Y)+m_\mu^2) - k\cdot k'(k\cdot p + k'\cdot p + m_N m_Y))$$
$$\times \frac{f_2^2}{(m_N+m_Y)^2}(-2k\cdot k'^2(k\cdot p + k'\cdot p - m_N m_Y) + k\cdot k'(2k\cdot p^2 - m_N m_Y(2k\cdot p + m_\mu^2)$$
$$+ 3k\cdot p m_\mu^2 - 2k'\cdot p^2 + k'\cdot p m_\mu^2 - 2k'\cdot p m_Y^2) + k\cdot p m_\mu^2(-2k\cdot p + 2k'\cdot p + m_Y(m_N+m_Y) - m_\mu^2))$$
$$\times g_1^2(k\cdot p(m_\mu^2 - m_Y(m_N+m_Y)) - k\cdot k'(k\cdot p + k'\cdot p - m_N m_Y))$$
$$\times \frac{f_1 f_2}{m_N+m_Y}(-2(k\cdot k' m_N(k\cdot p + k'\cdot p) - m_Y(k\cdot k' - k\cdot p)(k\cdot p - k'\cdot p) + k\cdot k' m_N m_Y^2 - k\cdot p m_N m_\mu^2))$$
$$\times f_1 g_1(2(k\cdot k'(k\cdot p - k'\cdot p) + k\cdot p(2k'\cdot p - m_\mu^2 + m_Y^2)))f_1 g_3(m_N m_\mu^2(k\cdot p - k\cdot k'))$$
$$\times \frac{f_2 g_1}{m_N+m_Y}(m_N(4k\cdot k'^2 + k\cdot k'(-2k\cdot p + 2k'\cdot p - 3m_\mu^2) + k\cdot p m_\mu^2)$$
$$- 2m_Y(k\cdot k' - k\cdot p)(k\cdot p + k'\cdot p) + 2k\cdot k' m_N m_Y^2)$$
$$\times \frac{f_2 g_3}{m_N+m_Y}(m_\mu^2(k\cdot p(m_Y(m_N-m_Y)+m_\mu^2) - k\cdot k'(k\cdot p + k'\cdot p + m_N m_Y)))\Big] \tag{A5}$$

$$\eta(Q^2,\vec{p}) = \frac{64}{m_Y}\Big[f_1^2(k\cdot k'(k\cdot p + k'\cdot p) - k\cdot p m_\mu^2)$$
$$\times \frac{f_2^2}{(m_N+m_Y)^2}((2(k\cdot k' - k\cdot p + k'\cdot p) - m_\mu^2)(k\cdot k'(k\cdot p + k'\cdot p) - k\cdot p m_\mu^2))$$
$$\times g_1^2(k\cdot k'(k\cdot p + k'\cdot p) - k\cdot p m_\mu^2)\frac{f_1 f_2}{m_N+m_Y}(2m_N(k\cdot k'(k\cdot p + k'\cdot p) - k\cdot p m_\mu^2))$$
$$\times f_1 g_1(2k\cdot k'(k'\cdot p - k\cdot p) + 2k\cdot p(m_\mu^2 - 2k'\cdot p))$$
$$\times f_1 g_3(m_\mu^2(k\cdot k' - k\cdot p)(m_N - m_Y))\frac{f_2 g_1}{m_N+m_Y}(-4k\cdot k'^2 m_N + k\cdot k'(2k\cdot p m_N - 2k'\cdot p m_N$$
$$+ m_\mu^2(3m_N + m_Y)) - k\cdot p m_\mu^2(m_N+m_Y))\frac{f_2 g_3}{m_N+m_Y}(k\cdot k' m_\mu^2(k\cdot p + k'\cdot p) - k\cdot p m_\mu^4)\Big] \tag{A6}$$

[1] N. Cabibbo, E. C. Swallow, and R. Winston, Annu. Rev. Nucl. Part. Sci. **53**, 39 (2003).
[2] J. M. Gaillard and G. Sauvage, Annu. Rev. Nucl. Part. Sci. **34**, 351 (1984).
[3] A. Garcia and P. Kielanowski, *The Beta Decay of Hyperons*, edited by A. Bohm, Lecture Notes in Physics Vol. 222 (Springer-Verlag, Berlin, 1985).
[4] O. Erriquez *et al.*, Phys. Lett. **B70**, 383 (1977).
[5] T. Eichten *et al.*, Phys. Lett. **B40**, 593 (1972).
[6] O. Erriquez *et al.*, Nucl. Phys. **B140**, 123 (1978).
[7] G. Fanourakis, L. K. Resvanis, G. Grammatikakis, P. Tsilimigras, A. Vayaki, U. Camerini, W. F. Fry, R. J. Loveless, J. H. Mapp, and D. D. Reeder, Phys. Rev. D **21**, 562 (1980).
[8] V. V. Ammosov *et al.*, Z Phys. C **36**, 377 (1987).
[9] V. V. Ammosov *et al.*, Pis'ma Zh. Eksp. Teor. Fiz. **43**, 554 (1986) [JETP Lett. **43**, 716 (1986)].
[10] J. Brunner *et al.* (SKAT Collaboration), Z. Phys. C **45**, 551 (1990).
[11] J. S. Bell and S. M. Berman, Nuovo Cimento **25**, 404 (1962).
[12] F. Chilton, Nuovo Cimento **31**, 447 (1964).
[13] S. L. Adler, Nuovo Cimento **30**, 1020 (1963).
[14] L. Egardt, Nuovo Cimento **29**, 954 (1963).
[15] N. Cabibbo and F. Chilton, Phys. Rev. **137**, B1628 (1965).
[16] A. Pais, Annals Phys. (Amsterdam) **63**, 361 (1971).
[17] R. E. Marshak, Riazuddin, and C. P. Ryan, *Theory of Weak Interactions in Particle Physics* (Wiley-Interscience, New York, 1969).
[18] C. H. Llewellyn Smith, Phys. Rep. **3**, 261 (1972).
[19] J. Finjord and F. Ravndal, Nucl. Phys. **B106**, 228 (1976).
[20] M. M. Block, Phys. Rev. Lett. **12**, 262 (1964).
[21] A. Sirlin, Nuovo Cimento **37**, 137 (1965).

[22] S. K. Singh and M. J. Vicente Vacas, Phys. Rev. D **74**, 053009 (2006).
[23] S. L. Mintz and L. Wen, Eur. Phys. J. A **33**, 299 (2007).
[24] S. L. Mintz and L. L. Wen, Nucl. Phys. **A766**, 219 (2006).
[25] K. S. Kuzmin and V. A. Naumov, Phys. At. Nucl. **72**, 1501 (2009).
[26] J. J. Wu and B. S. Zou, Few-Body Syst. **56**, 165 (2015).
[27] M. Rafi. Alam, M. Sajjad Athar, S. Chauhan, and S. K. Singh, J. Phys. G **42**, 055107 (2015); Phys. Rev. D **88**, 077301 (2013).
[28] http://www.fnal.gov/.
[29] http://j-parc.jp/index-e.html.
[30] H. Chen *et al.* (MicroBooNE Collaboration), Report No. FERMILAB-PROPOSAL-0974.
[31] O. Palamara (ArgoNeuT Collaboration), *Nucl. Phys. Proc. Suppl.* 217, 189 (2011).
[32] R. Acciarri *et al.* (DUNE Collaboration), arXiv:1512.06148.
[33] L. Fields *et al.* (MINERvA Collaboration), Phys. Rev. Lett. **111**, 022501 (2013).
[34] R. Acciarri *et al.* arXiv:1503.01520v1.
[35] R. Bradford *et al.*, *Nucl. Phys. Proc. Suppl.* 159, 127 (2006).
[36] S. Galster, H. Klein, J. Moritz, K. H. Schmidt, D. Wegener, and J. Bleckwenn, Nucl. Phys. **B32**, 221 (1971).
[37] S. Platchkov *et al.*, Nucl. Phys. **A510**, 740 (1990).
[38] V. Punjabi, C. F. Perdrisat, M. K. Jones, E. J. Brash, and C. E. Carlson, Eur. Phys. J. A **51**, 79 (2015).
[39] P. E. Bosted, Phys. Rev. C **51**, 409 (1995).
[40] H. Budd *et al.*, *Nucl. Phys. (Proc. Suppl.)* 139, 90 (2005).
[41] W. M. Alberico, S. M. Bilenky, C. Giunti, and K. M. Graczyk, Phys. Rev. C **79**, 065204 (2009).
[42] J. J. Kelly, Phys. Rev. C **70**, 068202 (2004).
[43] K. A. Olive *et al.* (Particle Data Group), Chin. Phys. C **38**, 090001 (2014).
[44] Y. Nambu, Phys. Rev. Lett. **4**, 380 (1960).
[45] L. Alvarez-Ruso, Y. Hayato, and J. Nieves, New J. Phys. **16**, 075015 (2014).
[46] J. G. Morfin, J. Nieves, and J. T. Sobczyk, Adv. High Energy Phys. **2012**, 1 (2012).
[47] H. Gallagher, G. Garvey, and G. P. Zeller, Annu. Rev. Nucl. Part. Sci. **61**, 355 (2011).
[48] K. L. Miller *et al.*, Phys. Rev. D **26**, 537 (1982).
[49] N. J. Baker *et al.*, Phys. Rev. D **23**, 2499 (1981).
[50] T. Kitagaki *et al.*, Phys. Rev. D **28**, 436 (1983).
[51] A. Bodek, M. E. Christy, and B. Coopersmith, Eur. Phys. J. C **74**, 3091 (2014).
[52] A. S. Meyer, M. Betancourt, R. Gran, and R. J. Hill, Phys. Rev. D **93**, 113015 (2016).
[53] V. Bernard, L. Elouadrhiri, and U. G. Meissner, J. Phys. G **28**, R1 (2002).
[54] V. Lyubushkin *et al.* (NOMAD Collaboration), Eur. Phys. J. C **63**, 355 (2009).
[55] A. A. Aguilar-Arevalo *et al.*(MiniBooNE Collaboration), Phys. Rev. D **88**, 032001 (2013); **81**, 092005 (2010); Phys. Rev. Lett. **100**, 032301 (2008).
[56] P. Adamson *et al.* (MINOS Collaboration), Phys. Rev. D **91**, 012005 (2015).
[57] R. Gran *et al.* (K2K Collaboration), Phys. Rev. D **74**, 052002 (2006).
[58] K. Abe *et al.* (T2K Collaboration), Phys. Rev. Lett. **116**, 181801 (2016); Phys. Rev. D **91**, 072010 (2015); **92**, 112003 (2015).
[59] Y. Nakajima *et al.* (SciBooNE Collaboration), Phys. Rev. D **83**, 012005 (2011).
[60] G. Cheng *et al.* (MiniBooNE and SciBooNE Collaborations), Phys. Rev. D **86**, 052009 (2012); M. O. Wascko (SciBooNE Collaboration), J. Phys. Conf. Ser. **136**, 042028 (2008).
[61] C. Wilkinson *et al.*, Phys. Rev. D **93**, 072010 (2016).
[62] A. M. Ankowski, O. Benhar, C. Mariani, and E. Vagnoni, Phys. Rev. D **93**, 113004 (2016).
[63] P. Stowell, S. Cartwright, L. Pickering, C. Wret, and C. Wilkinson, arXiv:1611.03275.
[64] S. M. Bilenky, *Basics of Introduction to Feynman Diagrams and Electroweak Interactions Physics* (Editions Frontieres, Gif-sur-Yvette Cedex, 1994).
[65] S. M. Bilenky and E. Christova, J. Phys. G **40**, 075004 (2013).
[66] S. M. Bilenky and E. Christova, Phys. Part. Nucl. Lett. **10**, 651 (2013).
[67] K. M. Graczyk, Nucl. Phys. **A748**, 313 (2005).
[68] N. Armenise *et al.*, Nucl. Phys. **B152**, 365 (1979).